STUDY of PLANAR STRATIFIED STRUCTURES and THEIR NOVEL APPLICATIONS : CHIRPED MIRRORS and PHOTONIC CRYSTALS

by

Emine Pınar Karabulut

A Thesis Submitted to the
Graduate School of Engineering
in Partial Fulfillment of the Requirements for
the Degree of

Master of Science

in

Electrical & Computer Engineering

Koç University

September, 2006

Koç University

Graduate School of Sciences and Engineering

This is to certify that I have examined this copy of a master's thesis by

Emine Pınar Karabulut

and have found that it is complete and satisfactory in all respects,
and that any and all revisions required by the final
examining committee have been made.

Committee Members:

_____

Prof. Irsadi Aksun

_____

Prof. Alphan Sennaroglu

_____

Assist. Prof. Alper Demir

_____

Assist. Prof. Hakan Urey

Date: _____

ABSTRACT

Study of Planar Stratified Structures and Their Novel Applications : Chirped Mirrors and Photonic Crystals

The main purpose of this work is to study and to investigate layered media, with a view of understanding its applications as chirped mirrors and photonic crystals. In this work, we reviewed the dispersion phenomena in general and investigated dispersion compensation role of chirped dielectric mirrors and used genetic algorithm for chirped mirror design. The other planar layered media, one dimensional photonic crystals are studied via plane wave method (PWM) which obtains dispersion diagram of the infinitely extended periodic planar structures and we propose a novel approach, namely generalized pencil of function (GPOF) approach, alternative to PWM. Similar to PWM, this approach finds dispersion characteristics of the photonic crystals. The main difference is that GPOF approach analyzes photonic crystals having finite number of layers which is more realistic. In addition, by this approach, one dimensional photonic crystal can be modeled with their homogeneous equivalents. The new approach is compared with PWM for the confirmation of accuracy. With this method, it is shown that homogeneous equivalents and dispersion characteristics can be found for oblique incident waves as well.

Keywords: planar layered media, chirped dielectric mirrors, dispersion compensation, genetic algorithm, photonic crystals, plane wave method, generalized pencil of function.

ÖZETÇE

Düzlemsel Katmanlı Yapıların Incelenmesi ve Yeni Uygulama Alanları: Chirped Aynalar ve Fotonik Kristaller

Çalışmanın ana amacı, fotonik kristal ve chirped aynalar gibi uygulama alanlarını gözlemleyerek düzlemsel yapıların çalışma prensiplerini incelemektir. Bu çalışma doğrultusunda yayılım görüngümünü gözden geçirip, chirped aynalar için yayılımı kompanse etme metodlarını inceledik ve genetik bir yayılım algoritması kullanarak yayılım karakterlerini inceledik. Diğer düzlemsel yapı olan tek boyutlu fotonik kristalleri ise, yayılım diyagramı oluşturan düzlem dalgaları yöntemini (DDY) kullanarak sonsuz periyodik yapılar için inceledik. Bu noktada, yeni bir alternatif yöntem olan GPOF yöntemi ile sonlu periyodik yapıların incelenmesini gerçekleştirdik. DDY ile paralel olarak GPOF yöntemi de düzlemsel yapıların yayılım karakterini bulmaktadır, aralarındaki ana fark, GPOF yönteminin, sonlu periyodik yapıları incelemesi ve böylece gerçek hayatta da uygulanabilecek sonuçları elde etmemizi sağlamasıdır. Aynı zamanda bu yeni yaklaşımla, fotonik kristaller, bu yapılara denk homojen yapılarla modellenebilmektedir. GPOF yöntemi sonuçlarını, DDY yöntemi sonuçları ile karşılaştırdık ve yeni geliştirilen GPOF yönteminin fotonik kristallerin yayılım karakterlerinin ve homojen yapı parametrelerinin bulunması için açılı dalgalar kullanılarak da uygulanabileceğini gösterdik.

Anahtar kelimeler: Düzlemsel katmanlı yapılar, chirped dielektrik aynalar, yayılımı kompanse etme, genetik algoritma, fotonik kristaller, düzlem dalgaları yöntemi, genelleştirilmiş fonksiyon kalemleri yöntemi (GPOF).

ACKNOWLEDGMENTS

I would like to thank my advisor, Professor Irsadi Aksun, who has been a great source of inspiration and patience and provided the right balance of suggestions, criticism, and freedom.

I would like to thank to Professor Alphan Sennaroglu for his appreciable help and comments.

Finally I thank my parents, my sister and my friends for providing me a morale support and optimism that helps me in hard days of my research.

TABLE OF CONTENTS

LIST OF FIGURES

Chapter 1

INTRODUCTION

For many years, researchers were provided with two primary means of understanding electromagnetic phenomena: measurements and analytical solutions. Measurements of electromagnetic systems bring direct result and physical intuition for the physical phenomena and the structures. However, the feasibility of fabricating new devices for each change in design can be time consuming and, depending on the application and the material, expensive. These two limitations, i.e., time and money, were often addressed by using analytical techniques, if possible, to predict electromagnetic behavior before the advent of computers. Improvements in computer memory and speed during the last few decades have allowed scientists/engineers to develop rapid and accurate analysis and design tools, and open the way of knowing the best numerically before entering the laboratory.

One of the structures for which computational analysis and design tools are crucial before manufacturing is layered medium. Planar layered media are the foundation of many structures used in microwave integrated circuits, antennas, laser technology and optics. The advantages of layered structures, such as their relatively less complicated manufacturing, low cost, light in weight, makes these structures very popular and resulting devices find many application areas in many rapidly growing fields, such as in laser physics. Today, in laser technology, short pulse generation is one of the main target of achievement which improves the rate and accuracy of data transfer. Because of the dominant role of soliton-like pulse shaping in ultrashort-pulse solid-state lasers [1], femtosecond-pulse generation relies on net negative, i.e. anomalous, intracavity group delay dispersion (GDD). Solid-state gain media always introduce a certain amount of frequency-dependent positive (normal) dispersion in the cavity, which must be balanced as well. Short pulse generation has advanced to a degree where the bandwidth of standard Bragg mirrors limits the bandwidth of ultra-short pulsed lasers. Chirped dielectric laser mirrors [2], which are nothing but planar layered media,

overcome this bandwidth limitation and they provide a powerful and compact technique for dispersion compensation. Additionally, they exhibit a broad high reflectance range while introducing a controlled negative group delay dispersion in femtosecond laser systems. The problem of designing broadband dielectric chirped mirrors for 10-fs or broadly tunable femtosecond solid-state laser systems is twofold. First, the mirrors have to have continuous high reflectivity over a broad spectral range without any drop in reflectivity regardless of wavelength. Second, the mirrors have to exhibit a smooth, possible negative variation of the group delay vs. frequency function over the whole operation range. Although it is quite simple to obtain reflection and transmission coefficients from a given multilayered planar structure, it is not as simple to achieve the two requirements of broadband dielectric chirped mirrors simultaneously, which can only be achieved by using a suitable optimization method. For this problem, a suitable optimization method needs to be capable of scanning a huge multi-dimensional solution space in multiple directions at once without a prior knowledge, which is the salient feature of Genetic optimization algorithms [3]. Genetic algorithms, as the name implies, were inspired by Darwin's theory of evolution, and therefore mimics the evolutionary process. Any genetic algorithm begins with a randomly selected set of solutions called population, and via probabilistic mutation and crossover operations defined over the population, a new generation (new solution set) is obtained. This is motivated by the hope that the new population will be better than the old ones. Actually, it is not only a hope, as the new generation is largely formed from the fittest members of the previous generation. The fitness of the members of the population can be quantified by a fitness function, which is referred to as cost function or penalty function in optimization nomenclatures, and based on the requirements of the problems. For example, for the design of a chirped mirror over a frequency band, fitness function is formed from the desired group delay dispersion and the required reflectivity in the range of frequency of interest. This procedure is repeated until the fitness values of the all population in one generation converge, or the fittest value from one generation to the next does not change significantly over a certain number of generations.

Devices that incorporate periodicity as a key feature of the design are also promising unrivaled performance in microwave circuits, antennas, fiber optics and laser technology. Periodic electromagnetic structures are commonplace in many of the item we rely on

everyday- from magnetron in microwave oven to ultraviolet radiation protection by polarized sunglasses. As first discussed by Yablonovitch [4] and John [5], photonic crystals are structures in which the refractive index is spatially periodic. The scale of the periodicity is of the same order of wavelength of the electromagnetic radiation. If properly tailored, the photonic crystal can exhibit a photonic band gap in which no light can propagate through the structure. This phenomenon is analogous to the case where the electron conduction is not allowed for some certain energy levels in a semiconductor. This analogy motivates the scientists and engineers to control the flow of light as they controlled electrons in a transistor and realize ultra-small optical devices such as single-mode LEDs [6],optical waveguides [7], frequency filters and nonlinear optical switches [8]. Furthermore, these optical devices may be combined to form one chip to create ultra-small optoelectronic integrated circuits, which is the new dream of scientists since the transistor has revolutionized the electronics.

The simplest form of the photonic crystals is the one with one-dimensional periodicity, which are made by stacking periodically alternating layers of different refractive index on top of each other. Researchers from the diverse fields of classical electromagnetics, solid-state physics, optics, material science, condensed matter physics, and semiconductor physics, are actively contributing to the base of electromagnetic crystal knowledge. A very powerful method to find the band structure of the crystal, known as plane wave expansion method, has been developed concurrently by Leung et al. [9], Zhang et al. [10],and Ho et al. [11]to solve for the eigenvalues of the governing homogenous operator equations obtained from Maxwell's equations in source-free, periodic structures extending to infinity in space. The main point of the method relies on the Bloch-Floquet theorem asserting that the eigenfunctions of the wave equation for a periodic potential are the product of a plane wave times a function with the periodicity of the lattice. It can yield accurate and reliable results, on the other hand, it requires intensive computation for complicated system involving thousands of plane waves. However, in this thesis, an alternative approach to plane wave method is proposed to obtain the dispersion characteristics, i.e., $\omega - k$-diagram, of the one dimensional photonic crystals, and is based on the generalized pencil of function (GPOF) method. As a by product, this approach provides an opportunity to model one dimensional photonic crystal with its homogeneous equivalent. The proposed method uses a set of reflection data taken from periodically alternating photonic crystal layers in order to fit them to a

number of complex exponentials via the GPOF method. Based on the fact that reflection coefficient expression from a homogenous slab forms a geometric series of the terms accounting for multiple reflections, which are exponential functions, one can deduce the effective wave number and equivalent permittivity and permeability of the homogenous slab from the approximated exponential terms. As a result, performing the same steps over a band of frequency of interest, the dispersion characteristics of the photonic crystal, as well as its equivalent homogenization parameters, can be obtained.

The main purpose of this work is to study and to learn layered media, with a view of understanding its applications as chirped mirrors and photonic crystals, and of possibly contributing either as improvement in their applications or as proposing new methods to help understand the working mechanisms of the structures. To achieve this goal, Chapter-2 reviews the background information about the general planar layered media, by providing the derivation of the governing equations starting from Maxwell's equations. Then, the definitions of the reflection and transmission coefficients are provided in a multilayered structures, by which one can obtain field distribution at any position in the structure.

Once the background materials are introduced, this is followed by the review of dielectric chirped mirrors in Chapter-3, where their need in short-pulse lasers and dispersion compensation characteristics are discussed. Then, the design of chirped mirrors, with the help of a genetic optimization algorithm, is explained, and some results are provided.

As another application of planar layered media, one dimensional photonic crystals is studied in Chapter-4. Before introducing the new numerical tools to analyze such structures, the photonic crystals in general are reviewed by plane wave expansion method to build intuition and to get reference data to validate the proposed methods. Then, a novel method to find the dispersion characteristics of finite periodic structures, and their equivalent homogenization parameters as the by-product of the method, is introduced with the necessary discussions on its theory and on its validation.

Chapter 2

PLANAR LAYERED MEDIA

2.1 Introduction

There are several advantages of multilayer media like having relatively simpler procedure for fabrication, and therefore easy to produce and cost effective and finding many application areas in microwave circuits, antennas and optics. Planar layered medium is the general name for one dimensional photonic crystals, dielectric mirrors in optics and printed structures in microwave and antenna applications. Therefore, it is necessary to begin with analyzing the layered media in a most general manner in order to understand the working mechanisms of photonic crystals and dielectric mirrors, which are explained in the following chapters. In this chapter, it is demonstrated that the vector wave equations for electric and magnetic fields can be reduced down to two scalar equation for a source-free and planar medium, with decoupled solutions referred to as transverse electric (TE) and transverse magnetic (TM) waves. Hence, by solving these equations, the propagation of waves through the layers of planar media. To do this, starting from Maxwell's Equations, we derive reflection coefficients, field amplitude coefficients and field expressions at any position of an n-layered planar medium for both TE and TM modes and at any angle of incidence.

2.2 Wave Equations for Electric and Magnetic Fields in Planar layered Media

A typical planar multilayer structure is demonstrated in Fig. 2.1, where the electromagnetic properties of isotropic layers, μ and ϵ, vary in one dimension only, which is assumed to be z-direction through out this chapter. In addition, the source layer is denoted by the script i, the origin of the coordinate system is defined at the source, the thickness, permittivity and permeability of any layer, layer-i for instance, are denoted by d_i, ϵ_i, and μ_i, respectively.

For the analysis of planar multilayer structures, we first need to write the governing differential equations starting from Maxwell's equations in isotropic and source-free region which for the sake of completeness given below:

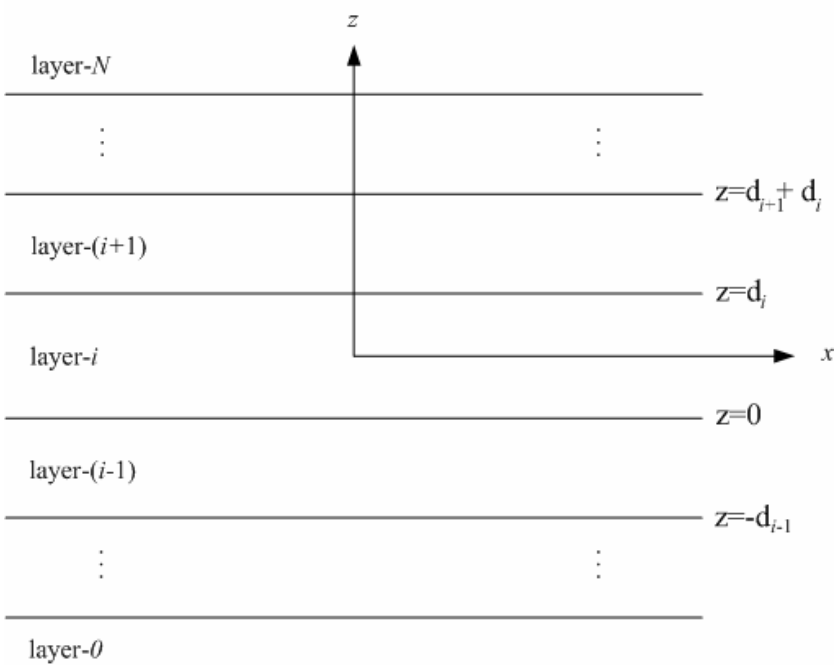

Figure 2.1: Multilayer planar medium

$$\nabla \cdot \epsilon(z)\vec{E}(\vec{r}) = 0 \tag{2.1}$$

$$\nabla \cdot \mu(z)\vec{H}(\vec{r}) = 0 \tag{2.2}$$

$$\nabla \times \vec{H}(\vec{r}) = j\omega\epsilon(z)\vec{E}(\vec{r}) \tag{2.3}$$

$$\nabla \times \vec{E}(\vec{r}) = -j\omega\mu(z)\vec{H}(\vec{r}) \tag{2.4}$$

After a few simple steps involving vector products and substitutions, the vector wave equations for electric and magnetic fields are obtained as:

$$\mu(z)\nabla \times \frac{1}{\mu(z)}\nabla \times \vec{E}(\vec{r}) - \omega^2\mu(z)\epsilon(z)\vec{E}(\vec{r}) = 0 \tag{2.5}$$

$$\epsilon(z)\nabla \times \frac{1}{\epsilon(z)}\nabla \times \vec{H}(\vec{r}) - \omega^2\mu(z)\epsilon(z)\vec{H}(\vec{r}) = 0 \tag{2.6}$$

For source-free cases, the vector wave equations can be separated to two independent scalar wave equations, which are characterized as the transverse electric (TE) and the transverse magnetic (TM) waves to z-direction. For TE_z formulation, although the electric field can be assumed to be linearly polarized in any direction in xy-plane, it can be assumed to be polarized in the direction of y-coordinate with no loss of generality, as the coordinate system can be rotated about z-axes to set the polarization of the field in y-direction only. Likewise, for TM_z case, only the y component of the magnetic field can be assumed to exist. Therefore the electric and magnetic fields for TE_z and TM_z modes, respectively can be defined as

For TE_z

$$\vec{E}(\vec{r}) = \hat{y}E_y(\vec{r}) \tag{2.7}$$

For TM_z

$$\vec{H}(\vec{r}) = \hat{y}H_y(\vec{r}) \tag{2.8}$$

Substituting the electric field (2.7) into the vector wave equation (2.5) as

$$\mu(z)\left[\left(\nabla\frac{1}{\mu(z)}\right)\times(\nabla\times\hat{y}E_y)+\frac{1}{\mu(z)}\nabla\times\nabla\times\hat{y}E_y\right]-\omega^2\mu(z)\epsilon(z)\hat{y}E_y=0$$

and using the fact that the permeability depends only on z-direction, the following expression can be abtained:

$$\mu(z)\left[\left(\frac{\partial}{\partial z}\mu(z)^{-1}\right)\hat{z}\times(\nabla\times\hat{y}E_y)+\frac{1}{\mu(z)}\nabla\times\nabla\times\hat{y}E_y\right]-\omega^2\mu(z)\epsilon(z)\hat{y}E_y=0$$

where the first triple vector product can be written as

$$\hat{z}\times(\nabla\times\hat{y}E_y)=\nabla(\hat{z}\cdot\hat{y}E_y)-(\hat{z}\cdot\nabla)\hat{y}E_y=\frac{\partial}{\partial z}\hat{y}E_y$$

$$\nabla\cdot\vec{D}=0\Rightarrow\nabla\cdot\epsilon(z)\hat{y}E_y=\nabla\epsilon(z)\cdot\hat{y}E_y+\epsilon(z)\nabla\cdot\hat{y}E_y=0\Rightarrow\nabla\cdot\hat{y}E_y=0$$

Note that the choice of the coordinate system has led us to the fields with no y variation. Hence, the vector wave equation (2.5) can be reduced to

$$\left[-\mu(z)\left(\frac{\partial}{\partial z}\mu(z)^{-1}\right)\frac{\partial}{\partial z}-\nabla^2-\omega^2\mu(z)\epsilon(z)\right]\hat{y}E_y=0$$

and, in addition, with the use of the product rule of derivative

$$\left(\frac{\partial}{\partial z}\mu^{-1}\right)\frac{\partial}{\partial z} \equiv \frac{\partial}{\partial z}\mu^{-1}\frac{\partial}{\partial z} - \mu^{-1}\frac{\partial^2}{\partial z^2}$$

it is further simplified to

$$\left[-\mu(z)\frac{\partial}{\partial z}\mu(z)^{-1}\frac{\partial}{\partial z} + \frac{\partial^2}{\partial z^2} - \nabla^2 - \omega^2\mu(z)\epsilon(z)\right]\hat{y}E_y = 0.$$

Since $\nabla \cdot \hat{y}E_y = \frac{\partial E_y}{\partial y} = 0$, the governing equation is finally obtained as

$$\left[\frac{\partial^2}{\partial x^2} + \mu(z)\frac{\partial}{\partial z}\mu(z)^{-1}\frac{\partial}{\partial z} + \omega^2\mu(z)\epsilon(z)\right]E_y = 0. \tag{2.9}$$

Similar procedure can be followed for the magnetic field and the following governing equation is also obtained

$$\left[\frac{\partial^2}{\partial x^2} + \epsilon(z)\frac{\partial}{\partial z}\epsilon(z)^{-1}\frac{\partial}{\partial z} + \omega^2\mu(z)\epsilon(z)\right]H_y = 0. \tag{2.10}$$

As mentioned before, the solutions of these two scalar wave equations,(2.9) and (2.10), are decoupled which can be demonstrated by finding the available field components corresponding to TE_z and to TM_z modes. We have assumed that with no loss of generality, E_y is the only electric field component for TE_z mode, and not a function of y. Hence, from Maxwell's equations, it can be shown that the following field components exist:

$$\nabla \times \hat{y}E_y = -j\omega\mu\vec{H}(x,z) \Rightarrow \vec{H}(x,z) = \hat{x}H_x(x,z) + \hat{z}H_z(x,z)$$

$$\nabla \times (\hat{x}H_x + \hat{z}H_z) = j\omega\epsilon\vec{E}(x,z) \Rightarrow \vec{E}(x,z) = \hat{y}E_y$$

For TM_z mode, the available field components are obtained by applying the same procedure to H_y:

$$\nabla \times \hat{y}H_y = j\omega\epsilon E_y(x,z) \Rightarrow \vec{E}(x,z) = \hat{x}E_x(x,z) + \hat{z}E_z(x,z)$$

$$\nabla \times (\hat{x}E_x + \hat{z}E_z) = -j\omega\mu\vec{H}(x,z) \Rightarrow \vec{H}(x,z) = \hat{y}H_y$$

Finally we have shown that the field components for TE_z and TM_z are mutually exclusive, decoupled (E_y, H_x, H_z) and (H_y, E_x, E_z), respectively.

So far we haven't taken into account the characteristics of the planar geometry in order to further simplify the scalar wave equations,(2.9) and (2.10). Notice in Fig. 2.1, the

geometry is unbounded in xy-plane and therefore there is no variation of the boundary on that plane which would force the magnitudes of the fields to vary, so the magnitudes must be constant. On the other hand, there should be a phase change along x-direction. Hence, the fields in such a geometry can be represented as follows:

$$E_y(x,z) = E_y(z)e^{\pm jk_x x} \tag{2.11}$$

$$H_y(x,z) = H_y(z)e^{\pm jk_x x} \tag{2.12}$$

The above argument is valid in every layer in a multilayer medium, the fields in all layers must have the same form as (2.11) and (2.12). On the other hand, boundary conditions dictate that the fields in all layers must have the same propagation constant in x-direction. This argument is called phase matching condition. Consequently, the scalar wave equations (2.9) and (2.10) are reduced down to one dimensional scalar wave equations:

For TE_z

$$\left[\mu(z)\frac{\partial}{\partial z}\mu^{-1}(z)\frac{\partial}{\partial z} + \underbrace{\omega^2\mu\epsilon - k_x^2}_{k_z^2}\right] E_y(z) = 0 \tag{2.13}$$

For TM_z

$$\left[\epsilon(z)\frac{\partial}{\partial z}\epsilon^{-1}(z)\frac{\partial}{\partial z} + \underbrace{\omega^2\mu\epsilon - k_x^2}_{k_z^2}\right] H_y(z) = 0 \tag{2.14}$$

Notice that the equations above can be separated and solved for each layer and then the complete geometry can be obtained by matching the boundary conditions at each interface between the layers. Hence, in the homogeneous medium of layer-i, these one dimensional scalar wave equations, (2.13) and (2.14), can be written as

For TE_z

$$\left[\frac{\partial^2}{\partial z^2} + \underbrace{\omega^2\mu_i\epsilon_i - k_x^2}_{k_{zi}^2}\right] E_{yi}(z) = 0 \tag{2.15}$$

For TM_z

$$\left[\frac{\partial^2}{\partial z^2} + \underbrace{\omega^2\mu_i\epsilon_i - k_x^2}_{k_{zi}^2}\right] H_{yi}(z) = 0 \tag{2.16}$$

So far, we have demonstrated that the fields in layered media, whose stratification is in z-direction and unbounded in the transverse dimensions, can be decomposed into independent

TE_z and TM_z waves and the field components of these waves are governed by (2.15) and (2.16). In order to find the general solution in medium, starting with the simplest form of a layered medium, two semi-infinite dielectric layers, is necessary for a better understanding of defining the reflection and transmission coefficients.

2.3 Fresnel's Reflection and Transmission Coefficients

One of the simplest layered geometry, two-medium one-interface structure, is shown in Fig. 2.2 in order to demonstrate the way to solve the scalar wave equation for TE_z waves.

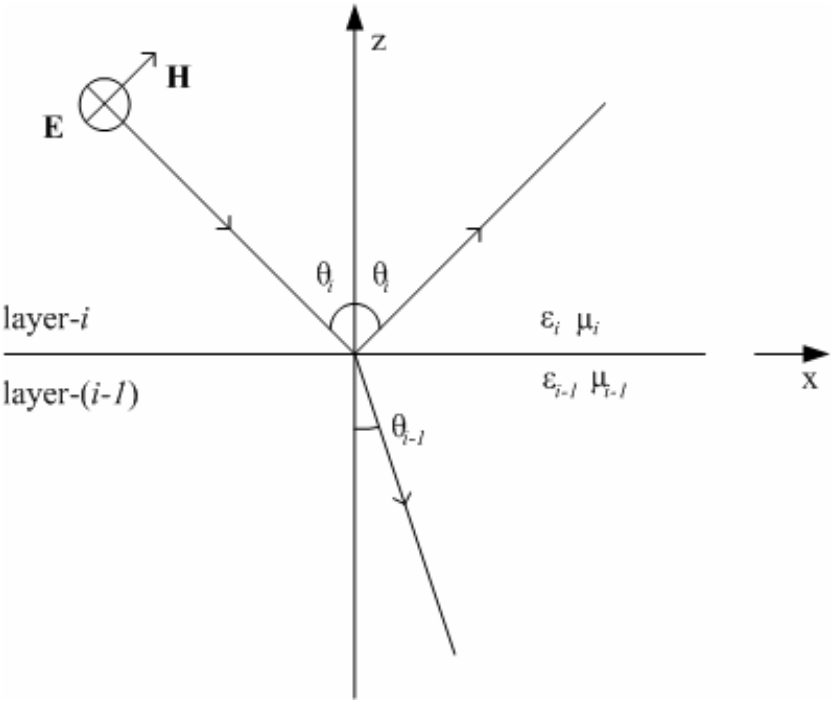

Figure 2.2: Two-layer medium showing incident,reflected and transmitted waves.

For layer-i, we have already found the scalar wave equation for TE_z waves (2.15) where $E_{yi}(x,z) = E_{yi}(z)e^{\pm jk_x x}$. Since the incident wave is assumed to propagate toward the positive x-direction in Fig. 2.2, the negative sign is chosen for the exponent of the x variation to represent the positive x-propagating wave. The electric fields in both layers as the solution of (2.15) and its similar formation for layer-(*i-1*), can be anticipated as

$$E_{yi}(z) = \underbrace{E_i^+ e^{-jk_{zi}z}}_{reflected} + \underbrace{E_i^- e^{+jk_{zi}z}}_{incident} \tag{2.17}$$

$$E_{y(i-1)}(z) = E_{i-1}^+ e^{-jk_{z(i-1)}z} + \underbrace{E_{i-1}^- e^{+jk_{z(i-1)}z}}_{transmitted} \tag{2.18}$$

where $k_{zi} = \sqrt{k_i^2 - k_x^2}$, $k_i = \omega\sqrt{\mu_i \epsilon_i}$ and there are four unknown to be determined. Considering layer-i, there is an incident wave propagating in negative z-direction and a reflected wave propagating in positive z-direction. Therefore, $E_i^- = E_0$ is the amplitude of the incident wave and it can be known by the source and E_i^+ must be the reflected part of the incident wave which is the reflection coefficient R times the amplitude of the incident wave. Since there is only transmitted wave propagating in negative z-direction, the coefficient of the positive propagating wave, E_{i-1}^+, must be equal to zero. Consequently, the electric field in both layers in (2.17) and (2.18) can be re-written as:

$$E_{yi}(z) = R_{i,i-1}^{TE} E_0 e^{-jk_{zi}z} + E_0 e^{+jk_{zi}z} \tag{2.19}$$

$$E_{y(i-1)}(z) = T_{i,i-1}^{TE} E_0 e^{+jk_{z(i-1)}z} \tag{2.20}$$

where $R_{i,i-1}^{TE}$ and $T_{i,i-1}^{TE}$ are the reflection and transmission coefficients for TE_z waves defined at the interface between layer-i and layer-*(i-1)*. Now we have two coefficients as unknowns and to determine these two coefficients we must consider the second boundary conditions that assures the continuity of the tangential magnetic fields at the interface. Hence, the tangential components of the magnetic fields are obtained by substituting the already obtained electric fields of the two layers, (2.19) and (2.20), into the Maxwell's equation as below:

$$\nabla \times \vec{E} = -j\omega\mu\vec{H} \Rightarrow \begin{cases} H_x = \frac{1}{j\omega\mu}\frac{\partial}{\partial z}E_y \\ H_z = -\frac{1}{j\omega\mu}\frac{\partial}{\partial x}E_y \end{cases} \tag{2.21}$$

$$H_{xi}(z) = \frac{k_{zi}}{\omega\mu_i} E_0 \left[e^{jk_{zi}z} - R_{i,i-1}^{TE} e^{-jk_{zi}z} \right] \tag{2.22}$$

$$H_{x(i-1)}(z) = \frac{k_{z(i-1)}}{\omega\mu_{i-1}} T_{i,i-1}^{TE} E_0 e^{+jk_{z(i-1)}z} \tag{2.23}$$

Implementing the boundary conditions on the continuity of the tangential electric and magnetic fields at the interface i.e., at $z = 0$, results in two equations for two unknowns:

$$1 + R^{TE}_{i,i-1} = T^{TE}_{i,i-1} \tag{2.24}$$

$$\frac{k_{zi}}{\mu_i}\left[1 - R^{TE}_{i,i-1}\right] = \frac{k_{z(i-1)}}{\mu_{i-1}} T^{TE}_{i,i-1} \tag{2.25}$$

Solving these equations simultaneously gives the reflection and transmission coefficients for TE_z waves in terms of the known quantities of the layers and these coefficients are called Fresnel's reflection and transmission coefficients:

$$R^{TE}_{i,i-1} = \frac{\mu_{i-1}k_{zi} - \mu_i k_{z(i-1)}}{\mu_{i-1}k_{zi} + \mu_i k_{z(i-1)}} \tag{2.26}$$

$$T^{TE}_{i,i-1} = \frac{2\mu_{i-1}k_{zi}}{\mu_{i-1}k_{zi} + \mu_i k_{z(i-1)}} \tag{2.27}$$

Similarly for TM_z waves, we must find the field expressions for H_{yi} and $H_{y(i-1)}$ since for this mode the governing differential equation is a scalar wave equation of H_y as (2.16). Similar procedure results in

$$H_{yi}(z) = R^{TM}_{i,i-1} H_0 e^{-jk_{zi}z} + H_0 e^{+jk_{zi}z} \tag{2.28}$$

$$H_{y(i-1)}(z) = T^{TM}_{i,i-1} H_0 e^{+jk_{z(i-1)}z} \tag{2.29}$$

where the reflection and transmission coefficients are defined for magnetic field. Using Maxwell's equations, the associated electric field is obtained as

$$\nabla \times \vec{H} = j\omega\epsilon\vec{E} \Rightarrow \begin{cases} E_x = -\frac{1}{j\omega\epsilon}\frac{\partial}{\partial z} H_y \\ E_z = \frac{1}{j\omega\epsilon}\frac{\partial}{\partial x} H_y \end{cases} \tag{2.30}$$

from which the tangential component of the electric field in both media can be written as

$$E_{xi}(z) = -\frac{k_{zi}}{\omega\epsilon_i} H_0 \left[e^{jk_{zi}z} - R^{TM}_{i,i-1} e^{-jk_{zi}z}\right] \tag{2.31}$$

$$E_{x(i-1)}(z) = -\frac{k_{z(i-1)}}{\omega\epsilon_{i-1}} T^{TM}_{i,i-1} H_0 e^{+jk_{z(i-1)}z}. \tag{2.32}$$

Implementing the boundary conditions on the continuity of the tangential components of the magnetic and electric fields results in the reflection and transmission coefficients for TM_z waves as

$$R_{i,i-1}^{TM} = \frac{\epsilon_{i-1}k_{zi} - \epsilon_i k_{z(i-1)}}{\epsilon_{i-1}k_{zi} + \epsilon_i k_{z(i-1)}} \tag{2.33}$$

$$T_{i,i-1}^{TM} = \frac{2\epsilon_{i-1}k_{zi}}{\epsilon_{i-1}k_{zi} + \epsilon_i k_{z(i-1)}} \tag{2.34}$$

Note that $T_{i,i-1} = 1 + R_{i,i-1}$ and $R_{i,i-1} = -R_{i-1,i}$ are valid for both TE_z and TM_z waves. After obtaining the general expressions for the Fresnel's reflection and transmission coefficients for two different polarizations in two semi infinite layers, it is time to generalize these expressions to any number of layer.

2.4 Generalized Reflection and Transmission Coefficients

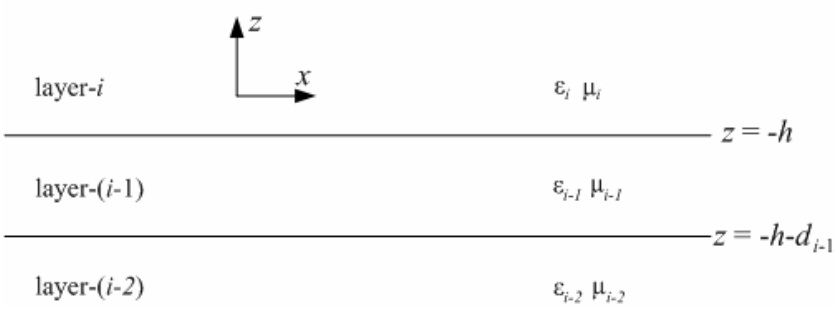

Figure 2.3: A typical three-layer planar geometry showing the coordinate system.

Between two semi-infinite layers, there is no multiple reflections involved which must be taken into account for layered media with more than one interface. To understand the most general multilayer geometry, it would be instructive to see the nature of multiple reflections in three-layer geometry first as in Fig. 2.3. Similar to the two-layer media, we assume source-free, homogeneous and isotropic layers in our analysis therefore the governing equations for TE_z and TM_z waves would have similar forms. Hence, for TE_z waves, the electric field in layer-i is as follows by inspection of (2.17).

$$E_{yi}(z) = A_i^{'} e^{jk_{zi}(z+h)} + B_i^{'} e^{-jk_{zi}(z+h)} \tag{2.35}$$

where $(z+h)$ is used to define the unknown coefficients, $A_i^{'}$ and $B_i^{'}$ at the interface between layer-i and layer-*(i-1)*. The amplitudes of down- and up-going waves at the interface ($z = -h$) are explicitly seen in the expressions as $A_i^{'}$ and $B_i^{'}$, respectively, and they are due to the multiple reflections from the interfaces of the top and bottom of the layer,respectively. Therefore, the ratio of $B_i^{'}/A_i^{'}$, can be defined as the generalized reflection coefficient and denoted by $\widetilde{R}_{i,i-1}^{TE}$. By using the generalized reflection coefficient ,the electric fields for TE_z can be rewritten for each layer as follows:

$$E_{yi}(z) = A_i \left[e^{jk_{zi}z} + \widetilde{R}_{i,i-1}^{TE} e^{-jk_{zi}z} e^{-jk_{zi}2h} \right] \tag{2.36}$$

$$E_{y(i-1)}(z) = A_{i-1} \left[e^{jk_{z(i-1)}z} + \widetilde{R}_{i-1,i-2}^{TE} e^{-jk_{z(i-1)}z} e^{-jk_{z(i-1)}2(-h-d_{i-1}} \right] \tag{2.37}$$

$$E_{y(i-2)}(z) = A_{i-2} e^{jk_{z(i-2)}z} \tag{2.38}$$

Notice that the reflection coefficient at the interface between layer-*(i-1)* and layer-*(i-2)* is just a simple Fresnel reflection coefficient since layer-*(i-2)*is the last interface so no multiple reflections occur. On the other hand, at the interface between layer-i and layer-*(i-1)*, the generalized reflection coefficient has to be derived. In order to find the unknown parameters, namely A_{i-1}, A_{i-2} and $\widetilde{R}_{i,i-1}^{TE}$, one needs to relate the down-going wave amplitude $atz = -h$ in layer-*(i-1)* to that in layer-i as

$$\begin{aligned} \underbrace{A_{i-1} e^{-jk_{z(i-1)}h}}_{down\ going\ wave\ in\ layer-(i-1)\ at\ z=-h} &= \\ \underbrace{A_i e^{-jk_{zi}h} T_{i,i-1}^{TE}}_{transmission\ of\ down-going\ wave\ in\ layer-i} &+ \\ \underbrace{A_{i-1} R_{i-1,i-2}^{TE} e^{jk_{z(i-1)}h} e^{jk_{z(i-1)}(-h-d_{i-1}} R_{i-1,i}^{TE}}_{reflection\ of\ up-going\ wave\ in\ layer-(i-1)\ at\ z=-h} & \end{aligned} \tag{2.39}$$

Hence, the amplitude of the down-going wave in layer-*(i-1)* is related to the amplitude of the incident wave in layer-i as follows

$$A_{i-1}e^{-jk_{z(i-1)}h} = A_i \frac{T^{TE}_{i,i-1}e^{-jk_{zi}h}}{1 - R^{TE}_{i-1,i-2}R^{TE}_{i-1,i}e^{-jk_{z(i-1)}2d_{i-1}}} \tag{2.40}$$

Simultaneously, the amplitude of the up-going wave in layer-i can be written as the sum of the amplitude of the reflected direct wave and the amplitude of the transmitted waves into layer-i from the op-going waves in layer-*(i-1)*:

$$\begin{aligned} \underbrace{A_i \widetilde{R}^{TE}_{i,i-1}e^{-jk_{zi}h}}_{up-going\,wave\,in\,layer-i\,at\,z=-h} &= \\ \underbrace{A_i R^{TE}_{i,i-1}e^{-jk_{zi}h}}_{reflection\,of\,down-going\,wave\,in\,layer-i\,at\,z=-h} &+ \\ \underbrace{A_{i-1}R^{TE}_{i-1,i-2}e^{jk_{z(i-1)}h}e^{jk_{z(i-1)}2(-h-d_{i-1})}T^{TE}_{i-1,i}}_{transmission\,of\,up-going\,wave\,in\,layer-(i-1)\,at\,z=-h} & \end{aligned} \tag{2.41}$$

Hence, the generalized reflection coefficient can be obtained, with the substitution of the amplitude transfer relation (2.40) as

$$\widetilde{R}^{TE}_{i,i-1} = R^{TE}_{i,i-1} + \frac{T^{TE}_{i,i-1}T^{TE}_{i-1,i}R^{TE}_{i-1,i-2}e^{-jk_{z(i-1)}2d_{i-1}}}{1 - R^{TE}_{i-1,i-2}R^{TE}_{i-1,i}e^{-jk_{z(i-1)}2d_{i-1}}} \tag{2.42}$$

Consequently, with the knowledge of the amplitude transfer (2.40) and the generalized reflection coefficient (2.42), the field components (2.36)-(2.38) can be defined by knowing the amplitude of the incident wave A_i specified by the source.

2.4.1 Extension to Multilayer Geometries:

Note that so far we have defined the amplitude transfer relation (2.40) and the generalized reflection coefficient (2.42) for the three-layer geometry. If the geometry is generalized to a geometry with multiple layers down below layer-*(i-2)* in Fig. 2.3, the Fresnel reflection coefficient $R^{TE}_{i-1,i-2}$ in (2.37) should be replaced by the generalized reflection coefficient to take into account the multireflections caused by the layers below. Hence replacing $R^{TE}_{i-1,i-2}$ by $\widetilde{R}^{TE}_{i-1,i-2}$ in (2.40) and (2.42) results in the following general definition for the amplitude transfer and the generalized reflection coefficient, defined at the interface layer-i and layer-*(i-1)* recursively:

$$A_{i-1}e^{-jk_{z(i-1)}h} = A_i \frac{T^{TE}_{i,i-1}e^{-jk_{zi}h}}{1 - \widetilde{R}^{TE}_{i-1,i-2}R^{TE}_{i-1,i}e^{-jk_{z(i-1)}2d_{i-1}}} \tag{2.43}$$

$$\widetilde{R}^{TE}_{i,i-1} = R^{TE}_{i,i-1} + \frac{T^{TE}_{i,i-1} T^{TE}_{i-1,i} \widetilde{R}^{TE}_{i-1,i-2} e^{-jk_{z(i-1)}2d_{i-1}}}{1 - \widetilde{R}^{TE}_{i-1,i-2} R^{TE}_{i-1,i} e^{-jk_{z(i-1)}2d_{i-1}}} \tag{2.44}$$

So far, only TE_z waves are considered and therefore all the reflection and transmission coefficients are of TE types. Since, the same analysis holds true for TM_z waves, the amplitude transfer relations and the generalized reflection coefficients for TM_z waves should be the same as those of TE_z waves, (2.43) and (2.44), provided that the reflection and transmission coefficients are replaced by TM types as (2.33) and (2.34).

In summary, this chapter gives a basic outlook to planar layered media. First we began with Maxwell equations for source-free planar media to reach vector-wave equations. Then we demonstrated that vector wave equations for electric and magnetic fields can be reduced down to two scaler equation with decoupled solutions referred to as transverse electric (TE) and transverse magnetic (TM). Then finally we took into account the characteristics of the planar geometry and defined direct reflection and transmission relations for each interface and multireflections at interfaces depending on the others for n-layered medium with any material specifications. Hence this analysis will give us the perspective to understand and interpret the nature of dielectric mirrors and photonic crystals in the following chapters of this thesis.

Chapter 3

CHIRPED MIRRORS

3.1 Introduction

One of the main trends of laser physics today is ultrafast laser technology. Since solid-state gain media always introduce a certain amount of frequency dependent positive dispersion in the cavity, in order to balance this, the femtosecond-pulse generation depends on a net negative intracavity group delay dispersion. Before the invention of chirped mirrors, brewster-angled prism pairs [12] built into the laser cavity were the only low-loss sources of broadband negative group delay dispersion. The problem inherent to these systems is increased pulsewidth sensitivity to cavity and prism alignment. In this systems, to maintain pulsewidth, even small cavity realignments necessitate subsequent readjustment of the prism positions and orientations which is quite time-consuming. To address this drawback, dispersion-controlled or chirped mirrors (CMs [2]) that offer broadband feedback and dispersion control in ultrafast laser systems by imparting negative dispersion over a broad spectral range are developed. These elements can permit generation of shorter, higher-quality pulses than previously achievable, while addressing the limitations of prism-controlled systems.

After their invention in 1994, dispersive dielectric multilayer media were rapidly improved and became the key components for mode-locked solid-state lasers, femtosecond parametric oscillators, chirped pulse amplification systems and pulse compressors due to the advantages above and their relatively broader operation range. A chirped mirror is a kind of dielectric mirror which is usually used for dispersion compensation or sometimes just as a mirror with particularly large reflection bandwidth. The basic idea of chirped mirror designs is that the Bragg wavelength is not constant but varies within the structure, so different wavelengths penetrate to a different extend into the mirror structure and thus experience a different delay in time. However, a design directly based on this idea would experience strong oscillations of the group delay or even more of the higher order dispersions. Therefore chirped dielectric mirrors are improved by some optimization techniques

and many design approaches were further developed such as double chirped mirrors (DCMs [13, 14]), back-side coated chirped mirrors (BASIC [15]), tilted-front-interface mirrors (TFI [16]) and brewster-angled chirped mirrors [17] to achieve requisite dispersion and reflection features between desired bandwidth.

In the following sections of this chapter, we review the dielectric chirped mirrors together with the explanation of the dispersion concept in general and the reason why a net negative group delay dispersion is necessitated for dispersion compensation in the cavity of the laser. Then, in the last section of the chapter, the design of chirped mirrors, with the help of a genetic optimization algorithm, is explained, and some results are provided.

3.2 Theory

The phenomenon of signal distortion caused by a dependence of phase velocity on frequency is called dispersion. For a plane wave in a lossless medium the phase velocity is constant i.e. independent of frequency. However in some cases; in a lossy dielectric medium for instance; waves of different frequencies propagate with different phase velocities and then signal disperses. The main reason why the phase velocity depends on frequency originates from the fact that the refractive index of the medium is a function of frequency of the traveling wave.This dependence of the refractive index on frequency or similarly on wavelength has two effects on a pulse, one in space which is angular dispersion and the other in time called chirp as in upper and lower sections of Fig.3.1, respectively. Both of these effects play major roles in ultrafast optics.

Since different frequency components of light propagate with different phase velocities, such a signal comprises a "group" of frequencies and forms a wave packet. The group velocity is the velocity of propagation of the wave packet envelope and the formula for computing the group velocity in a dispersive medium is as follows:

$$V_g = \frac{d\omega}{dk} \tag{3.1}$$

Now, the angular frequency ω is the same in or out of the medium, but $k = k_0 n$, where k_0 is the k-vector in vacuum, and n is medium dependent refractive index. So it's easier to think of ω as the independent variable:

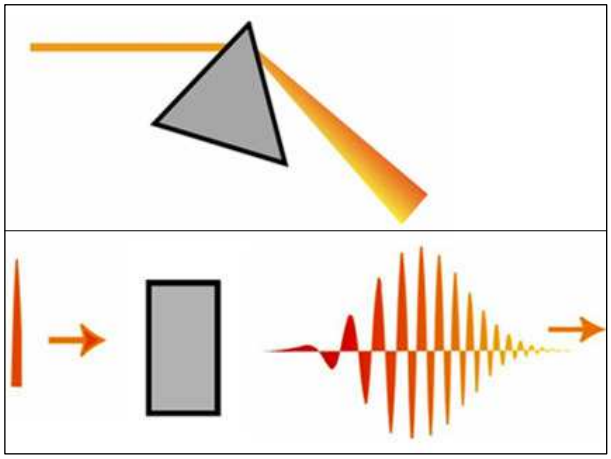

Figure 3.1: *First Figure:* The angular dispersion caused by the existence of the different refraction angles for different wavelengths of the light. *Second Figure:* The dispersion in time caused by the different refractive index for different wavelengths. The velocity of different wavelengths of light varies and the waves reach a specific point at different times.

$$V_g = \left[\frac{dk}{d\omega}\right]^{-1} \tag{3.2}$$

Using $k = \frac{\omega}{c} n(\omega)$, where c is speed of light in vacuum, we can find

$$\frac{dk}{d\omega} = \frac{1}{c}\left[n + \omega\frac{dn}{d\omega}\right]$$

and,

$$V_g = \frac{c}{n}\frac{1}{\left[1 + \frac{\omega}{n}\frac{dn}{d\omega}\right]}.$$

Since $V_{phase} = \frac{c}{n}$, we can express group velocity in terms of V_{phase} as

$$V_g = \frac{V_{phase}}{\left[1 + \frac{\omega}{n}\frac{dn}{d\omega}\right]}. \tag{3.3}$$

Note that phase velocity is equal to group velocity when $\frac{dn}{d\omega} = 0$ such as in vacuum, as expected. For $\frac{dn}{d\omega} > 0$ i.e. for increasing n with ω, $V_g < V_{phase}$ which means that high frequency components of the wave travel with a relatively lower velocity. This phenomenon, namely normal dispersion, occurs in frequency regions called non-absorbing regions. On the contrary, if n decreases with ω ($\frac{dn}{d\omega} < 0$) then $V_g > V_{phase}$. This kind of dispersion is called anomalous dispersion and occurs in the absorbing regions. This time, the high frequency components travel faster compared to waves propagating with lower frequency. In addition,

we more often consider the refractive index in terms of wavelength so one can write the group velocity in terms of the vacuum wavelength λ_0 by using the chain rule

$$\frac{dn}{d\omega} = \frac{dn}{d\lambda_0}\frac{d\lambda_0}{d\omega}$$

and knowing that $\lambda_0 = 2\pi c/\omega$ equation 3.3 is rewritten as

$$V_g = \frac{V_{phase}}{\left[1 - \frac{\lambda_0}{n}\frac{dn}{d\lambda_0}\right]}. \tag{3.4}$$

In addition we can define group index N_g as

$$V_g = \frac{c}{n}\frac{1}{\left[1 - \frac{\lambda_0}{n}\frac{dn}{d\lambda_0}\right]} = \frac{c}{N_g}.$$

where

$$N_g = n - \lambda\frac{dn}{d\lambda}. \tag{3.5}$$

Note that $\frac{dn}{d\lambda}$ is negative in most regions (normal regions), therefore $N_g > n$ except in regions of anomalous dispersion.

If a signal or pulse containing more than one wavelength, the individual components of this signal will travel at different group velocities in dispersive media. These components will reach the receiver at different times, effectively stretching out the time which takes for a signal to arrive. This effect is called group velocity dispersion.

Consider an optical pulse with a finite spectral bandwidth $\Delta\lambda$, traveling through a dispersive medium. The time required to travel a distance L is called the latency

$$\tau = \frac{L}{c}N_g(\lambda) \tag{3.6}$$

where the spectral width of the pulse spans from λ_1 to λ_2 i.e. $\Delta\lambda = |\lambda_1 - \lambda_2|$. Each wavelength component will propagate at a slightly different speed. We know that if medium exhibit normal dispersion, then $\frac{dn}{d\lambda} < 0$ which means that , for instance, $\lambda_{red} > \lambda_{blue} \Longrightarrow n_{red} < n_{blue}$. Therefore, it is clear that $N_{g,red} < N_{g,blue}$. Hence, (3.6) implies that more time is required to travel a distance L for blue light compared to the red light, i.e, $\tau_{red} < \tau_{blue}$, so, for a wave having different waves with different wavelengths faces a pulse spread. In the time domain, this pulse spread will be

$$\Delta\tau = \frac{L}{c}(N_g(\lambda_1) - N_g(\lambda_2)) = \frac{L}{c}\Delta N_g = \frac{L}{c}\frac{dN_g}{d\lambda}\Delta\lambda$$

Since we already know the group index expression in terms of wavelength as (3.5), we can take its derivative as follows

$$\frac{dN_g}{d\lambda} = \frac{d}{d\lambda}\left[n - \lambda\frac{dn}{d\lambda}\right] = \frac{dn}{d\lambda} - \frac{dn}{d\lambda} - \lambda\frac{d^2n}{d\lambda^2} = -\lambda\frac{d^2n}{d\lambda^2}$$

and finally pulse spread can be rewritten

$$\Delta\tau = -\frac{L}{c}\lambda\frac{d^2n}{d\lambda^2}\Delta\lambda \tag{3.7}$$

Note that pulse spreading depends on second derivative of material index and group velocity dispersion comes from that expression. The term

$$D = \frac{\lambda}{c}\frac{d^2n}{d\lambda^2} \tag{3.8}$$

is called material dispersion or group velocity dispersion and usually specified in units of ps/km of length per nm bandwidth.

Note that, we find for normal dispersive media, high frequency components travel slower than the lower frequency components and for anomalous dispersive media the situation is reversed. Therefore, if a pulse composed of different frequency components enters a normal dispersive medium, the lower frequencies leave the medium first and the highest frequencies leave after a while. Then we have a dispersed wave i.e. the pulse is distorted. If we can manage to design a medium showing right anomalous dispersion characteristics and let this dispersed pulse enter our designed medium, the high frequencies will travel faster than low frequency ones. On the other hand, since the low frequency components have reached the anomalous dispersive medium earlier because of the first medium, the dispersion can be manipulated and the sharp pulse can be regained. Indeed, the idea explained here is the focal point of the dispersion compensation methods using chirped mirrors.

So far we've reached an expression for group velocity dispersion related to the second derivative of the wavelength dependent refractive index. Now it is time to find the same relation between second derivative of the index and spectral phase. Since, second derivative of the refractive index of a dispersive medium can not be found directly in practice, it is necessary to relate the wavelength dependent dispersion to a value which can be derived or

measured from a medium in reality. In the following section, it will be derived that spectral phase of the wave due to the dispersive media has the same expression of (3.8) containing the second derivative of the refractive index of the medium.

3.2.1 Spectral Phase and Dispersive Optical Devices

The effect of a linear passive optical devices (lenses,prisms,mirrors etc.) on a pulse is multiplication of the frequency-domain field by the transfer function of the optical medium as follows

$$\vec{E}_{out}(\omega) = H(\omega)\vec{E}_{in}(\omega) \tag{3.9}$$

Here $H(\omega)$ is the transfer function of the medium such as $H(\omega) = A_H(\omega)e^{-j\phi_H(\omega)}$. Fig. 3.2 shows the transfer relation of the incoming wave passing through a medium or an optical device.

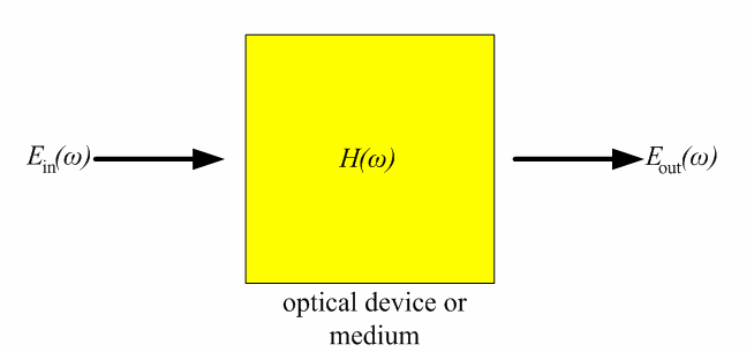

Figure 3.2: The medium or an optical device as a transfer region for the input wave $\vec{E}_{in}(\omega)$. The resulting output wave $\vec{E}_{out}(\omega)$ depends on the transfer properties $\vec{H}(\omega)$ of the medium.

Since we can also write $\vec{E}_{in}$ and $\vec{E}_{out}$ in a similar manner, the spectral phase of the output wave will be obtained simply by adding the spectral phases.

$$\phi_{out}(\omega) = \phi_H(\omega) + \phi_{in}(\omega) \tag{3.10}$$

According to (3.10) one can simply control the output spectral phase by adjusting the medium phase $\phi_H(\omega)$ by the knowledge of $\phi_{in}(\omega)$ where

$$\phi_H(\omega) = n(\omega)k_0L = k(\omega)L \tag{3.11}$$

To account for dispersion, expand the phase (k-vector) in a Taylor series such as

$$k(\omega)L = k(\omega_0)L + k'(\omega_0)[\omega - \omega_0]L + \frac{1}{2}k''(\omega_0)[\omega - \omega_0]^2L + ... \tag{3.12}$$

The first two terms are all related to important quantities namely phase velocity and group delay in equations below

$$k(\omega_0) = \frac{\omega_0}{V_{phase}(\omega_0)} \tag{3.13}$$

$$k'(\omega_0) = \frac{1}{V_g(\omega_0)} \tag{3.14}$$

(3.14) can be simply derived by (3.1). The third term shows the variation in propagation velocity with frequency since it is further derivation of the second such as

$$k''(\omega) = \frac{d}{d\omega}\left[\frac{1}{V_g}\right] \tag{3.15}$$

which means that the group velocity will be different for different wavelengths in the pulse. Remember that in previous section we discussed the same argument and pointed out that different wavelengths travel with different velocities causing a pulse spread in time. It will be more illuminating if we calculate $k''(\omega)$ in terms of wavelength as follows: Recall that

$$\frac{d\lambda_0}{d\omega} = -\frac{\lambda_0^2}{2\pi c}$$

$$\frac{d}{d\omega} = \frac{d\lambda_0}{d\omega}\frac{d}{d\lambda_0} = -\frac{\lambda_0^2}{2\pi c}\frac{d}{d\lambda_0}$$

and rewrite group velocity expression (3.3) as

$$V_g = \frac{c}{n - \lambda_0\frac{dn}{d\lambda_0}}$$

Thus $k''(\omega)$ is

$$\begin{aligned}
\frac{d}{d\omega}\left[\frac{1}{V_g}\right] &= -\frac{\lambda_0^2}{2\pi c}\frac{d}{d\lambda_0}\left[\frac{1}{c}\left(n - \lambda_0\frac{dn}{d\lambda_0}\right)\right] \\
&= -\frac{\lambda_0^2}{2\pi c^2}\frac{d}{d\lambda_0}\left[n - \lambda_0\frac{dn}{d\lambda_0}\right] \\
&= -\frac{\lambda_0^2}{2\pi c^2}\left[\frac{dn}{d\lambda_0} - \lambda_0\frac{d^2n}{d\lambda_0^2} - \frac{dn}{d\lambda_0}\right]
\end{aligned} \tag{3.16}$$

Simplifying this expression yields

$$k''(\omega) = \frac{\lambda_0^3}{2\pi c^2}\frac{d^2n}{d\lambda_0^2} \tag{3.17}$$

in unit of ps^2/km, which is directly related to group velocity dispersion (3.8) such that

$$D = \frac{2\pi c}{\lambda_0^2}k''(\omega_0) \tag{3.18}$$

In addition, we can define delays in terms of the velocities and the length of the medium L and this brings us to group delay dispersion concept. The phase delay:

$$k(\omega_0) = \frac{\omega_0}{V_{phase}(\omega_0)} \Rightarrow t_{phase} = \frac{L}{V_{phase}(\omega_0)} = \frac{k(\omega_0)L}{\omega_0} \tag{3.19}$$

The group delay:

$$k'(\omega_0) = \frac{1}{V_g(\omega_0)} \Rightarrow t_g = \frac{L}{V_g(\omega_0)} = k'(\omega_0)L \tag{3.20}$$

Note that, the group delay (3.20) and the latency (3.6) give exactly the same expression and define the required time of waves to travel distance L. The group delay dispersion (GDD):

$$k''(\omega) = \frac{d}{d\omega}\left[\frac{1}{V_g}\right] \Rightarrow GDD = \frac{d}{d\omega}\left[\frac{1}{V_g}\right]L = k''(\omega)L \tag{3.21}$$

which is in units of fs^2 or ps^2. Remember (3.7), (3.21) includes information about the pulse spread in time propagating through a dispersive medium. Recall that we expand the spectral phase of the optical medium,H, in a Taylor series:

$$\phi_H(\omega) = \phi_{H0} + \phi_{H1}[\omega - \omega_0] + \frac{1}{2}\phi_{H2}[\omega - \omega_0]^2L + ... \tag{3.22}$$

and we do the same for spectral phase of the pulse:

$$\phi(\omega) = \phi_0 + \phi_1[\omega - \omega_0] + \frac{1}{2}\phi_2[\omega - \omega_0]^2L + ... \tag{3.23}$$

So, to manipulate light we must add or subtract spectral phase term. For instance to eliminate the linear chirp (second order spectral phase), we must design an optical device whose second order spectral phase cancels that of the pulse

$$\phi_2 + \phi_{H2} = 0$$

i.e.

$$\frac{d^2\phi}{w\omega^2}|_{\omega_0} + \frac{d^2\phi_H}{w\omega^2}|_{\omega_0} = 0$$

If ϕ_2 is the pulse second-order spectral phase entering a medium, and $k''L$ is the second-order spectral phase of the medium, then the resulting pulse second-order phase will be the sum: $\phi_2 + k''L$.

If ϕ_{H2} is positive, a positively chirped pulse will broaden further, a negatively chirped pulse will be shortened. Usually the medium, in laser environment for instance, up chirps i.e. positively chirps the pulse. Therefore, we need a way of generating negative GDD to compensate pulse spread. This is an important process because pulses spread further and further as they propagate through materials. As mentioned before, dispersive dielectric mirrors (chirped mirrors) are commonly used optical media for applications necessitating negative GDD to compensate spread of the positively chirped signal. In [18], an ultra-broadband chirped mirror is proposed with a high reflectivity ($R > 99\%$) from 660 to $1060nm$ for normal incidence by a computer optimization. This specific design is composed of alternating layers of SiO_2 and TiO_2 as the low and high-index materials, respectively, with optical thicknesses varying around a quarter of $800nm$. Fig. 3.3 shows the reflectivity characteristics of the design.

In addition to the high reflectivity, the resulting design has an average negative GDD of $-50fs^2$. The considerable extension of high reflectivity range of the chirped mirrors can be achieved at the expense of the higher fluctuation in the negative GDD. Fig. 3.4 shows the slight deviation of the phase of the design from the ideal phase having constant negative GDD of $-50fs^2$.

In this work we focused on the design method for building such mirrors having negative GDD and high reflectivity in a specified range of frequency. Therefore, in order to design such mirrors, the optimization tool must have the ability to manipulate these two parameters simultaneously. In addition, those mirrors are usually composed of more than 50 layers whose thicknesses have to be determined. Therefore, the space of all potential solutions is truly huge and it must be explained in multiple directions at once. On the other hand, we have not a specific initial guesses i.e. any prior knowledge of the thicknesses to begin the optimization. These arguments force us to select genetic algorithm (GA) as optimization tool to design such mirrors and GA satisfies all these abilities explained above.

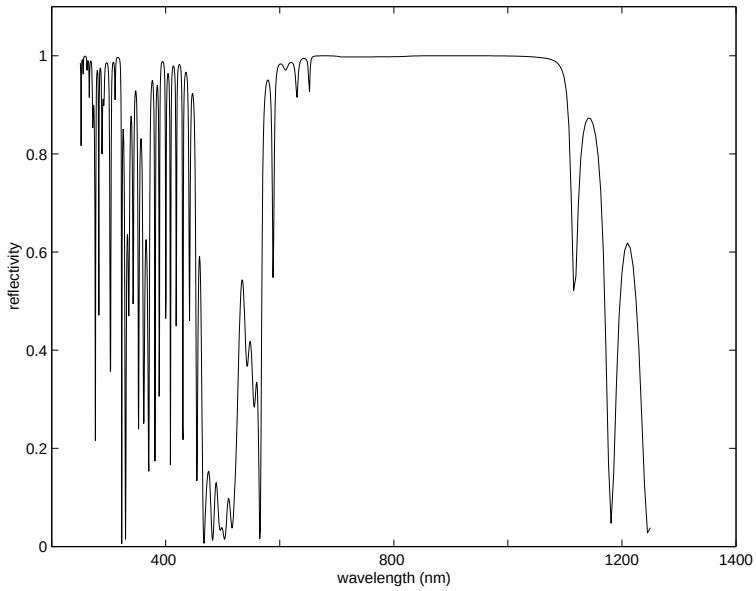

Figure 3.3: Reflectivity of the ultra-broadband CM vs. wavelength. Optical thicknesses of the design are specified as in [18]. $S : substrate$, $n_S = 1.51$; $A : air$, $n_A = 1.0$; high and low index materials are TiO_2 and SiO_2, respectively, at $\lambda = 790nm$ with indices $n_H = 2.315$, $n_L = 1.45$.

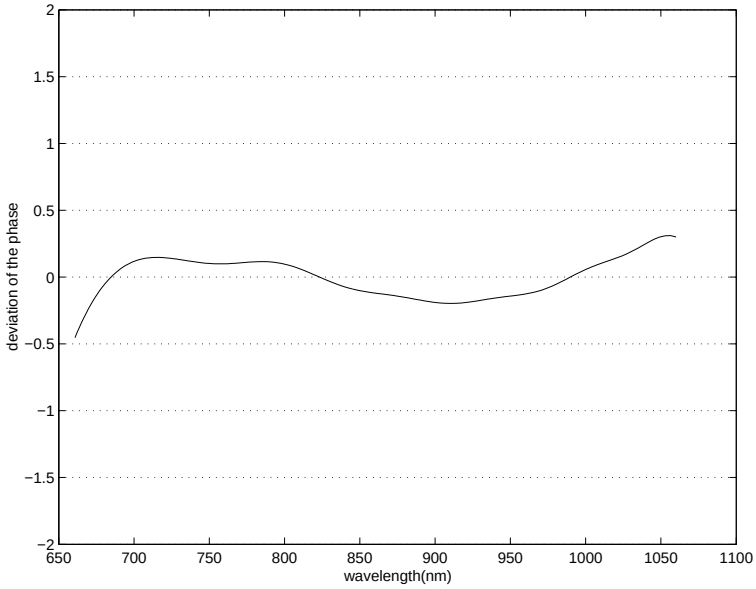

Figure 3.4: The deviation of the phase from the ideal phase having constant group delay dispersion vs wavelength. The design details are taken from [18].

GA finds the optimum thickness value for each layer knowing which materials are going to be used (refractive indices of materials) and in which frequency range this mirror operates.

3.3 Method and Design: Genetic Algorithm as an Optimization Tool and Its Adaptation to Mirror Design

"Genetic algorithms are based on a biological metaphor: They view learning as a competition among a population of evolving candidate problem solutions. A 'fitness' function evaluates each solution to decide whether it will contribute to the next generation of solutions. Then, through operations analogous to gene transfer in sexual reproduction, the algorithm creates a new population of candidate solutions [23]." Concisely stated, a genetic algorithm is a programming technique that mimics biological evolution as a problem-solving strategy.

Let us explain the strategy of the algorithm by considering our main design problem. As discussed before, these optimization tools maintain and manipulate a family or a population of solutions and implement a survival of the fittest strategy in its search for better solution. In our case, the population is composed of individuals which are the thicknesses of the mirror's layers. Initially many individual solutions are randomly generated to form an initial population. The population size depends on the nature of the problem, but typically contains several hundreds or thousands of possible solutions. Traditionally, the population is generated randomly, covering the entire range of possible solutions (the search space). For a 50-layer mirror, the thickness of each layer for every individuals is randomly selected between $10nm$ and $250nm$. Then, during each successive epoch, a proportion of the existing population is selected to breed a new generation. Individual solutions are selected through a fitness-based process, where fitter solutions (as measured by a fitness function) are typically more likely to be selected. Fitness function for our purpose determine two properties of the individual. First one is the reflectivity characteristics of the current mirror which must be greater than 99%. Secondly, the GDD of the medium must be both negative and non-fluctuating as much as possible. Once selection has chosen fit individuals, they must be randomly altered in hopes of improving their fitness for the next generation. There are two basic strategies to accomplish this. The first and simplest is called mutation. Just as mutation in living things changes one gene to another, so mutation in a genetic algorithm

causes small alterations at single points in an individual's code. Here mutation is made by randomly changing a thickness value of a layer belonging to an individual. The second method is called crossover, and entails choosing two individuals to swap segments of their code, producing artificial "offspring" that are combinations of their parents. This can be achieved by interchanging one part of the thickness sequence of an individual with complementary one of an other individual. By producing a "child" solution using the above methods of crossover and mutation, a new solution is created which typically shares many of the characteristics of its "parents". New parents are selected for each child, and the process continues until a new population of solutions of appropriate size is generated.This generational process is repeated until a termination condition has been reached. Here, when fixed number of generations is reached, optimization is terminated.

Fig. 3.5 represents an example for the result of an dielectric mirror optimization via genetic algorithm. The materials used for the alternating layers are selected from the reference [18] which is given as an example in previous section. As it is seen, the resulting design propose high reflectivity ($R > 99.7\%$) from 660 to 1060 nm and an average negative GDD of $-70fs^2$. The deviation of the phase from one with a constant $-70fs^2$ GDD and GDD itself are represented.

Note that, since we must consider two criteria which are the high reflectivity and smooth negative GDD, the design algorithm has unavoidable tradeoff. In order to reduce the fluctuations of the GDD, we must sacrifice the reflectivity and reduce it to some reasonable level or to obtain a nearly ideal 100% reflectivity, we must allow some fluctuation of the GDD.

In this chapter we explained the dispersion phenomena in general for any lossy media and then the origin of the negative GDD required to compensate the dispersion in the laser cavity. In addition, we discussed the method which we have used to design the chirped mirrors. Then, starting the example given in [18], we have designed a chirped mirror composed of the same dielectric materials and same number of layers. In order to obtain further improvement for the smoothness of GDD and/or in order to extend the usage of the chirped mirror for wider bandwidth, one must require the optimization process having more population size and much more generations. This can be achieved by using higher speed computer with higher memory. As future work, the current design will be improved by extending its bandwidth and reducing the fluctuations of GDD via high performance

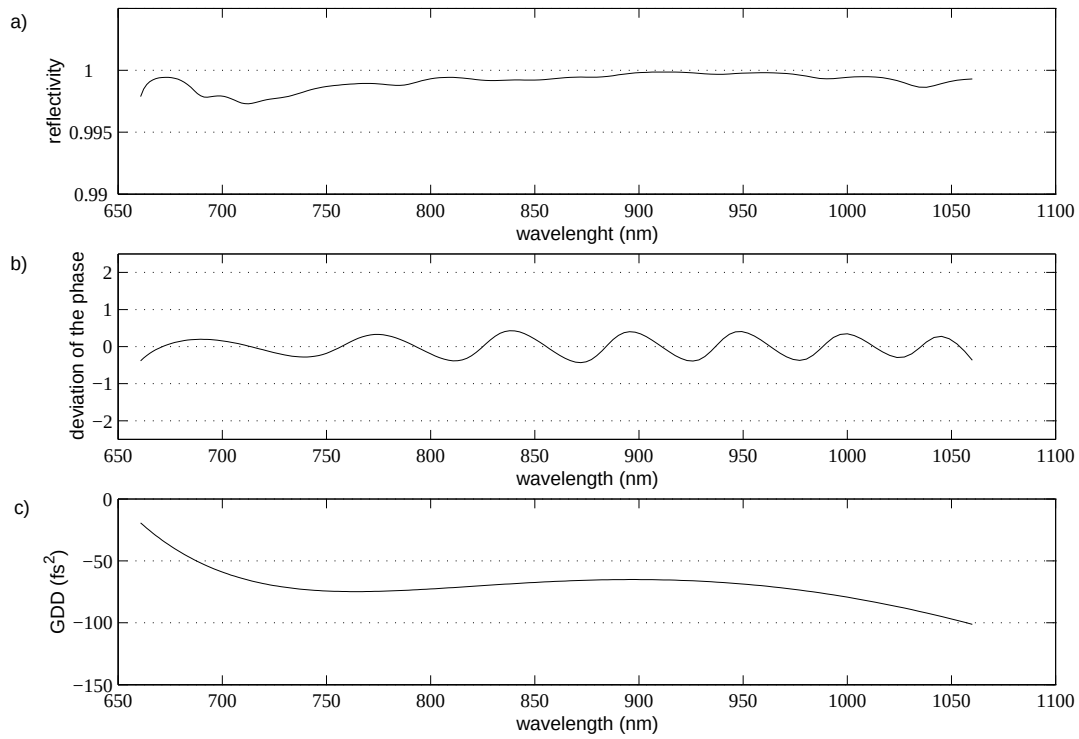

Figure 3.5: The reflectance (a), phase deviation (b) and GDD (c) of an ultra-broadband dielectric chirped mirror designed via genetic algorithm vs. wavelength. The refractive indices of the substrate, low index material (SiO_2), high index material (TiO_2), ambient(air) are 1.51, 1.45, 2.315 and 1, respectively, at $\lambda = 790nm$.

computer facility.

Chapter 4

PHOTONIC CRYSTALS

4.1 Introduction

Photonic band-gap materials, also referred to as electromagnetic band-gap (EBG) materials, electromagnetic crystals(EC) or photonic crystals (PhC), are inhomogeneous structures composed of periodic regions of materials. These materials are able to localize electromagnetic wave or more specifically light in specified areas by preventing it from propagating in certain directions as first proposed by E. Yablonovitch [4] and S. John [5].

Electromagnetic wave propagation in a photonic band-gap material is analogous to electron conduction in semiconductors. The validity of Bloch-Floquet's theorem for Maxwell equations implies the existence of photonic bands and allowed and forbidden frequency regions for light propagation, in analogy to electrons in crystalline solids. According to the solid state theory, it is known that semiconductors allow electron conduction only for electrons that have energies within a specific range, often called band-gap. Similarly for photonic band-gap materials, electromagnetic wave propagation is possible only for some frequency range and is forbidden for some another range which is called photonic band-gap. The band and gap properties depend on the permittivity, dimensions of the structure and angle of incidence. Photonic band-gap materials can be categorized according to the number of direction in which the periodicity takes place. In one-dimension such structures are easy to imagine and can be made with relative ease by stacking alternating layers of different refractive index on top of each other. The interest in such a multilayer is that it displays high reflectivity for light of which the wavelength matches the periodicity of the Bragg reflector (1-D photonic crystal). This property was discovered many years ago before people thought about photonic crystals. Nowadays, such Bragg mirrors are used in many optical applications that require high reflectivity. By selecting the right materials, one can easily make mirrors that are better than metal mirrors in a specific wavelength range. On the other hand, for two and three dimensional photonic crystals we must arrange

the contrasting dielectrics in a lattice that is periodic along two and three axes, respectively (see Fig. 4.1). Two-dimensional crystals may be realized by fabricating regular arrays of pillars or by drilling a regular pattern of holes in a substrate and they are used especially in optical communication as photonic crystal fibers [19]-[22]. These materials received also a lot of attention because of their possible use in integrated optics, where they might be used to control and manipulate the flow of light in an (essentially planar) optical chip. In such two-dimensional applications the devices mainly use the reflective properties of the photonic crystal to guide, steer or wavelength select the light. Since the periodicity of the photonic crystal is on the order of the wavelength of light these devices can be substantially smaller than existing solutions that make use of normal optical components such as mirrors, gratings, ring resonators or cavities. Eventually the goal of such devices is to make integrated circuits that combine both electronic functions and optical functions. From a fundamental point of view three-dimensional photonic crystals are the most interesting objects to study. If the right crystal structure is chosen and if the index contrast is sufficient a material can be designed that does not allow light within a certain frequency range to propagate in the crystal in any possible direction. In this special case, Bragg reflection will occur in any possible direction and the light cannot propagate into the crystal. This is what is known as a full photonic bandgap and has important consequences. One of those consequences is that if one would place a light source inside such a crystal, the light emitted cannot escape from the crystal. As a result the energy will be stored forever in the coupled system of the light source and the photonic crystal.

In this chapter, starting from Maxwell's equations, the propagation of light in photonic crystals and plane wave method (PWM) are described. The plane wave method is used to find the allowable frequencies for light propagation in all crystal directions and calculate the field distributions for any frequency of light assuming that the dimensions and periodicity of the crystal extend to infinity. In the last part of the chapter,we will discuss more realizable examples of photonic band gap materials which are one dimensional crystals having finite number of layers and state the differences between analysis methods of finite-layered and the ideal 1D photonic crystal cases.

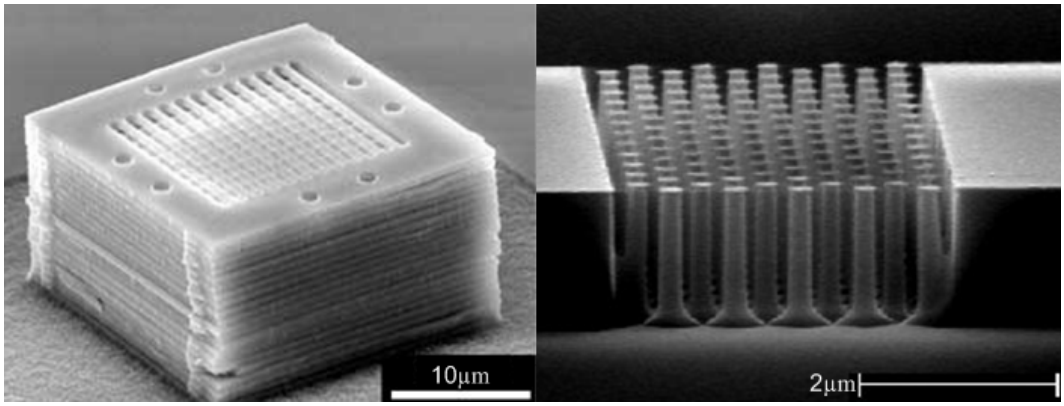

Figure 4.1: *Left:* Three dimensional photonic crystal.[24] *Right:* Two dimensional photonic crystal.[25]

4.2 Methods and Analysis of One and Two Dimensional Photonic Band Gap Materials

4.2.1 Analysis of One Dimensional Photonic Band Gap Materials via Plane Wave Method

We begin our study of photonic crystals with the simplest possible case: a one dimensional system. In order to understand the propagation of light in 1-D photonic crystals, we use the principle of electromagnetism with symmetry concept and see the important features of the photonic crystals such as photonic band gaps. This part explains the general ideas about PWM, Hermitian systems, symmetry, variational theorem etc. and leads us to more complicated photonic band-gap structures in other parts of this chapter.

In order to analyze and present the electromagnetic wave propagation in all possible states through a photonic crystal, free charges and current should not exist in the system. In addition, restricting the structure to lossless (relative permittivity is real), linear (permittivity is independent of electric field) and nonmagnetic medium ($\mu = \mu_0\mu_r$ where $\mu_r = 1$) with no frequency dependence of the dielectric function, the resulting Maxwell's equations become:

$$\nabla \cdot \epsilon_0 \, \epsilon_r(\vec{r}) \, \vec{E}(\vec{r}, t) = 0 \tag{4.1}$$

$$\nabla \cdot \mu_0 \, \vec{H}(\vec{r}, t) = 0 \tag{4.2}$$

$$\nabla \times \vec{E}(\vec{r},t) = -\mu_0 \frac{\partial \vec{H}(\vec{r},t)}{\partial t} \tag{4.3}$$

$$\nabla \times \vec{H}(\vec{r},t) = \epsilon_0\, \epsilon_r \frac{\partial \vec{E}(\vec{r},t)}{\partial t} \tag{4.4}$$

Where $\epsilon_r(\vec{r})$ is periodic with the same periodicity of the photonic crystal geometry. Since Maxwell's equations are linear, we can expand them into a set of harmonic modes (according to $e^{j\omega t}$ time dependence) and then separate out the time dependence. After substituting Faraday's and Ampere's equations into the other, the problem reduced to two vectorial eigenvalue equations called master equations as follows:

$$\frac{1}{\epsilon(\vec{r})}\left[\nabla \times \nabla \times \vec{E}(\vec{r})\right] = \frac{\omega^2}{c^2}\vec{E}(\vec{r}) \tag{4.5}$$

$$\nabla \times \left[\frac{1}{\epsilon(\vec{r})}\nabla \times \vec{H}(\vec{r})\right] = \frac{\omega^2}{c^2}\vec{H}(\vec{r}) \tag{4.6}$$

Master equations together with transverse conditions $\nabla \cdot \epsilon(\vec{r})\vec{E}(\vec{r}) = 0$ and $\nabla \cdot \vec{H}(\vec{r}) = 0$ completely determine the modes $\vec{E}(\vec{r})$ and $\vec{H}(\vec{r})$ for a given frequency and from master equations we can find the optical band structures.

Our aim is to solve these two vectorial operator equations, whose operators are $\frac{1}{\epsilon(\vec{r})}\left[\nabla \times \nabla \bullet\right]$ and $\nabla \times \left[\frac{1}{\epsilon(\vec{r})}\nabla \bullet\right]$, to be able to predict the behavior of light in the photonic crystal. Here (4.6) is very important for our aim. This operator is a special type of one known as Hermitian operator. What it means for an operator to be Hermitian? An operator let say $\boldsymbol{\Theta}$ is Hermitian if $(\vec{F}, \boldsymbol{\Theta}\vec{G}) = (\boldsymbol{\Theta}\vec{F}, \vec{G})$ for any vector fields $\vec{F}(\vec{r})$ and $\vec{G}(\vec{r})$. That is it does not matter which function is operated upon before taking the inner product (the definition of inner product and the proof of why the eigenoperator is Hermitian are in appendix).

General properties of the Hermitian modes:

1. The Hermitian operator $\boldsymbol{\Theta}$ must have real eigenvalues.

2. Since $\epsilon(\vec{r})$ is positive everywhere, all of the eigenvalues must be positive.

3. The Hermiticity of $\boldsymbol{\Theta}$ forces any two harmonic modes $\vec{H}_1$ and $\vec{H}_2$ with different frequencies f_1 and f_2 to have an inner product of zero.

(The proof of the properties are in appendix.)

Since ω_1 and ω_2 are different frequencies, $(\vec{H}_1, \vec{H}_2) = 0$ i.e. they are orthogonal modes. If two harmonic modes have equal frequencies then we say they are degenerate and they are not necessarily orthogonal. However since $\mathbf{\Theta}$ is a linear operator, any linear combination of these degenerate modes is itself a mode with the same frequency.

In addition, there exists a simpler way to understand some qualitative features of harmonic modes which is called the variational theorem. Basically, according this theorem, the mode tends to concentrate its displacement energy in regions of high dielectric constants while remaining orthogonal to the modes below it in frequency due to the Hermiticity. The variational energy is as below:

$$E_f = \frac{1}{2(\vec{H}, \vec{H})} \int \frac{1}{\epsilon(\vec{r})} \left| \frac{\omega}{c} \vec{D} \right| \tag{4.7}$$

From this expression we can see that E_f is minimized when the displacement field $\vec{D}$ is concentrated in the region of high dielectric constant. To minimize E_f , a harmonic mode will therefore tend to concentrate its displacement field in regions of high dielectric so its frequency is reduced [26]. (The derivation of (4.7) is in appendix.)

In summary;

- Our all possible fields that can propagate in photonic crystal are solutions (eigenstates) of master equation.
- All states are orthogonal to each other if they are not degenerate modes.
- Since the eigenoperator is linear, any linear combinations of states are also solutions of the master equation.
- To minimize their energy, they tend to localize their displacement field in high ϵ regions while keeping them orthogonal to each other.

In the following section we solve these eigenequations for one dimensional photonic crystal structures.

4.2.2 Solution of the One Dimensional Master Equation by PWM

The simplest example of a photonic crystal is a one-dimensional array of dielectric slabs in air (see Fig. 4.2). When we consider waves propagating in $+z$ direction, from symmetry property of the crystal the fields propagating through the slabs must be the function of z only. Because xy-plane extends to infinity, there is no physical difference between two coordinates on this plane and there can not exist fields propagating in the direction of propagation . Therefore field components can be written an follows:

$$\vec{E} = E_x(z)\hat{x} + E_y(z)\hat{y} \tag{4.8}$$

$$\vec{H} = H_x(z)\hat{x} + H_y(z)\hat{y} \tag{4.9}$$

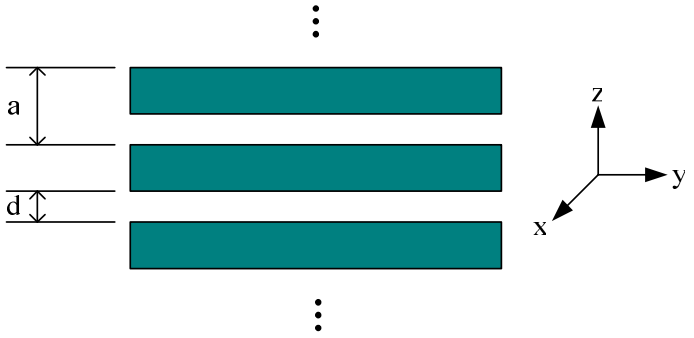

Figure 4.2: One dimensional photonic crystal consisting of air slabs of width d and dielectric slabs with periodicity a namely lattice constant.

By substituting the above fields into the master equations 4.5 and 4.6, one dimensional versions of the master equations are obtained:

$$\frac{1}{\epsilon_r(z)}\frac{\partial^2 E_{x,y}(z)}{\partial z^2} = -\frac{\omega^2}{c^2}E_{x,y}(z) \tag{4.10}$$

$$\frac{\partial}{\partial z}\left[\frac{1}{\epsilon_r(z)}\frac{\partial H_{x,y}(z)}{\partial z}\right] = -\frac{\omega^2}{c^2}H_{x,y}(z) \tag{4.11}$$

where $\epsilon_r(z) = \epsilon_r(z+a)$ i.e. periodic with the crystal lattice.

Here we will validate (4.11) because of its Hermitian characteristics after solving both master equation. In order to find the solution we must use the periodicity and symmetry

features of the geometry and that will brings us to the concept famous on the solid state physics namely Bloch-Floquet's theorem. Bloch-Floquet's theorem asserts that the eigenfunctions of the wave equation for a periodic potential are the product of a plane wave times a function with the periodicity of the crystal lattice. With the light of this theorem, the field propagating through 1-D photonic crystal can be written as:

$$H_{x,y}(z) = \sum_{n}^{H} e^{j\frac{2\pi nz}{a}} e^{jk_z z} = e(z)e^{jk_z z} \tag{4.12}$$

In order to understand the theorem, we must begin with the property of translational symmetry of the periodic structure. We know that the system exhibit discrete translational symmetry in z-direction which means that the system is invariant under the translational operator $\mathbf{T_a}$ shifting the system by amount of periodicity a. For instance, the relative permittivity function itself is invariant under $\mathbf{T_a}$ such that $\mathbf{T_a}\epsilon_r(z) = \epsilon_r(z+a) = \epsilon_r(z)$. Since discrete translation is symmetry of our system, it does not matter whether we operate with an arbitrary Hermitian operator $\mathbf{\Theta}$ or we first invert the coordinates, then operate with $\mathbf{\Theta}$, and then change them back. Therefore the relation below holds:

$$\mathbf{\Theta} = \mathbf{T_a^{-1}\Theta T_a} \tag{4.13}$$

This equation can be rearranged as:

$$\mathbf{T_a\Theta} - \mathbf{\Theta T_a} = 0 \tag{4.14}$$

We have shown that our system is symmetric under discrete translation only if the translation operation and eigenoperator satisfy (4.14). If we now operate any mode of the system $\vec{H}(r)$ we obtain

$$\mathbf{T_a}(\mathbf{\Theta}\vec{H}) - \mathbf{\Theta}(\mathbf{T_a}\vec{H}) = 0 \tag{4.15}$$

and

$$\mathbf{\Theta}(\mathbf{T_a}\vec{H}) = \mathbf{T_a}(\mathbf{\Theta}\vec{H}) = \frac{\omega^2}{c^2}(\mathbf{T_a}\vec{H}). \tag{4.16}$$

From this relation, we can say that if $\vec{H}$ is a harmonic mode with frequency ω, and then $\mathbf{T_a}\vec{H}$ is also a mode with frequency ω. If there is no degeneracy then there can only be one mode per frequency so $\vec{H}$ and $\mathbf{T_a}\vec{H}$ can be different only by a multiplicative factor α:

$\mathbf{T_a}\vec{H} = \alpha\vec{H}$. In other words, any state must satisfy the inversion property which is itself an eigenequation. Then what sort of field is an eigenfunction of the operator $\mathbf{T_a}$? We can prove that a mode with the form e^{jkz} as an eigenfunction of $\mathbf{T_a}$ in z-direction:

$$\mathbf{T_a}e^{jkz} = e^{jk(z+a)} = (e^{jka})e^{jkz} \tag{4.17}$$

The corresponding eigenvalue is e^{jka}. Notice that we don't have different eigenvalues for all different k. For each k, $k+2\pi/a$ and $k+m2\pi/a$ for any integer m has the same eigenvalue. Indeed, all modes with wave vectors $k + m(2\pi/a)$ where m is an integer, constitute a degenerate set. Amplifying k by an integral multiple of $a = 2\pi/a$ leaves the state unchanged. We call $\vec{a} = a\hat{z}$ the primitive reciprocal lattice vector.

Since any linear combination of these degenerate eigenfunctions is itself an eigenfunction with the same eigenvalue, we can take linear combinations of our original modes to put them in the form

$$H_k = \sum_m C_m e^{j(k+\frac{2\pi m}{a})z} = e^{jkz}\sum_m C_m e^{j\frac{2\pi m}{a}z} = h(z)e^{jkz} \tag{4.18}$$

where C's are expansion coefficients and $h(z)$ is a periodic function in z, such that $h(z) = h(z + a)$. As you see from translational symmetry concept, we have reached (4.12). From this relation, we can see the fields, propagating in a photonic crystal, from a different point of view. These fields may be thought as a plane wave propagating in free space (uniform) but being modulated by a periodic function because of the periodic lattice [27].

On the other hand, since the modes of wave vectors k and $k + m2\pi/a$ are not different from a physical point of view, it is sufficient to analyze the system only in the region between $-\pi/a < k < \pi/a$. This region is called as Brillouin zone. In addition, because of the time reversal symmetry, the Brillouin zone can be reduced to $0 < k < \pi/a$ which is called irreducible Brillouin zone. (The details about time reversal symmetry are in appendix.)

So far we manage to express the field by sum of plane waves according to Bloch-Floquet's theorem. On the other hand, in order to solve master equation (4.11), inverse relative permittivity function must also be defined by plane waves. This is achieved by Fourier series since the permittivity is a periodic function along the photonic crystal as well.

$$\frac{1}{\epsilon_r(z)} = \sum_m C_m^{\epsilon} e^{j\frac{2\pi m}{a}z} \tag{4.19}$$

When the field and permittivity expressions, (4.18) and (4.19), are substituted into the master equation (4.11), the eigenvalue equation is obtained.

$$\frac{\partial}{\partial z}\left[\sum_m C_m^{\epsilon} e^{j\frac{2\pi m}{a}z}\frac{\partial}{\partial z}\sum_n C_n^H e^{j(k+\frac{2\pi n}{a})z}\right] = -\frac{\omega^2}{c^2}\sum_m C_m^H e^{j(k+\frac{2\pi m}{a})z} \tag{4.20}$$

$$\begin{aligned}\sum_n\left(k+\frac{2\pi n}{a}\right)C_n^H\sum_m\frac{2\pi m}{a}C_m^{\epsilon}e^{j\frac{2\pi(m+n)}{a}z}e^{jkz} \quad &+\\ \sum_n\left(k+\frac{2\pi n}{a}\right)^2 C_n^H\sum_m C_m^{\epsilon}e^{j\frac{2\pi(m+n)}{a}z}e^{jkz} \quad &=\\ \frac{\omega^2}{c^2}\sum_m C_m^H e^{j(k+\frac{2\pi m}{a})z} &\end{aligned} \tag{4.21}$$

In order to simplify the summation, (4.21) is reorganized by substituting m-n instead of m (infinite summation allows us to do so). After reorganizing the terms, the summation becomes:

$$\begin{aligned}\sum_n\left(k+\frac{2\pi n}{a}\right)C_n^H\sum_m\frac{2\pi(m-n)}{a}C_{m-n}^{\epsilon}e^{j\frac{2\pi m}{a}z}e^{jkz} \quad &+\\ \sum_n\left(k+\frac{2\pi n}{a}\right)^2 C_n^H\sum_m C_{m-n}^{\epsilon}e^{j\frac{2\pi m}{a}z}e^{jkz} \quad &=\\ \frac{\omega^2}{c^2}\sum_m C_m^H e^{j(k+\frac{2\pi m}{a})z} &\end{aligned} \tag{4.22}$$

So we reach more simplified form for our eigenequation such that:

$$\sum_n\left(k+\frac{2\pi n}{a}\right)\left(k+\frac{2\pi m}{a}\right)C_{m-n}^{\epsilon}C_n^H = \frac{\omega^2}{c^2}C_m^H \tag{4.23}$$

This relation forms an eigenvalue problem by taking the integers m and n symmetric around zero. For instance when $m = n = 3$ $(-1\,0\,1)$ the problem becomes:

$$\begin{bmatrix} \left(k-\frac{2\pi}{a}\right)\left(k-\frac{2\pi}{a}\right)C_0^{\epsilon} & (k)\left(k-\frac{2\pi}{a}\right)C_{-1}^{\epsilon} & \left(k+\frac{2\pi}{a}\right)\left(k-\frac{2\pi}{a}\right)C_{-2}^{\epsilon} \\ \left(k-\frac{2\pi}{a}\right)(k)C_1^{\epsilon} & (k)(k)C_0^{\epsilon} & \left(k+\frac{2\pi}{a}\right)(k)C_{-1}^{\epsilon} \\ \left(k-\frac{2\pi}{a}\right)\left(k+\frac{2\pi}{a}\right)C_2^{\epsilon} & (k)\left(k+\frac{2\pi}{a}\right)C_1^{\epsilon} & \left(k+\frac{2\pi}{a}\right)\left(k+\frac{2\pi}{a}\right)C_0^{\epsilon} \end{bmatrix}\begin{bmatrix} C_{-1}^H \\ C_0^H \\ C_1^H \end{bmatrix} = \begin{bmatrix} C_{-1}^H \\ C_0^H \\ C_1^H \end{bmatrix} \tag{4.24}$$

The above relation forms an ordinary eigenvalue problem like $Ax = \lambda x$. After solving the problem, the eigenvalues $\frac{\omega^2}{c^2}$ and eigenvectors (eigenstates) C_n^H are obtained. In order to find the eigenvalues and vectors, one must construct the matrix A, so the only remaining problem is to find the dielectric Fourier coefficients, which are obtained by inverse Fourier transform.

$$C_n^H = \int_{-a/2}^{a/2} \frac{1}{\epsilon(z)} e^{-j\frac{2\pi n}{a}z} dz \tag{4.25}$$

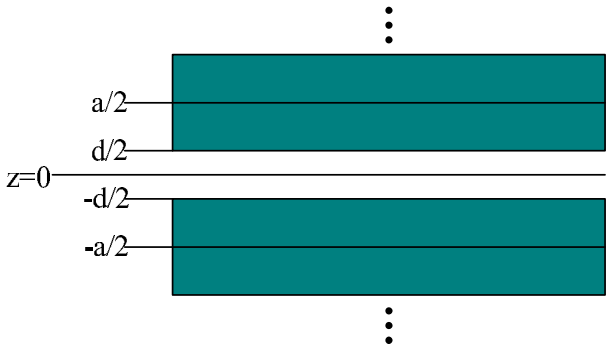

Figure 4.3: Proper references of z-coordinate for the inverse Fourier transform integration.

If we take $z = 0$ point in the middle of the air slab as in Fig. 4.3, the unit cell should be divided into three regions for integration. The resulting Fourier coefficients of inverse dielectric function, where ϵ is dielectric function of the lattice, take the form below.

$$C_n^H = \left(1 - \frac{1}{\epsilon_r}\right) \frac{d}{a} sinc\left(\frac{\pi n d}{a}\right) + \frac{1}{\epsilon_r}\delta \tag{4.26}$$

All information is now available to solve the matrix A for the eigenvalues. Fig. 4.4 shows the band structure for the photonic crystal with a lattice constant 1 and the air slab 0.8. The dielectric constant is taken as 13. Band structure is formed by solving eigenequation for each k value taken with equal intervals between $-2\pi/a$ and $2\pi/a$ and plotted k values and its corresponding eigenvalues i.e frequencies. In more complicated cases, the band diagram is plotted only in Brillouin zone.

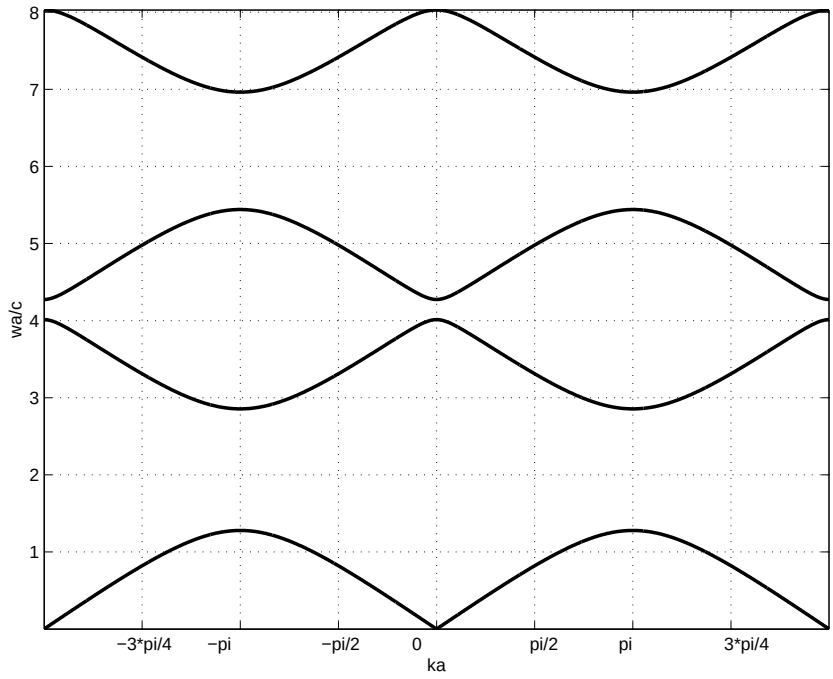

Figure 4.4: Band structure of 1D photonic crystal for H field. Lattice constant is $a = 1$, the thickness of the air slab in one period is $d = 0.8a$ with dielectric $\epsilon = 13$.

4.2.3 The origin of photonic band gap

The gap between bands $n = 1$ and $n = 2$ occurs at the edge of the Brillouin zone at $k = \pi/a$ (see Fig. 4.5). We can consider dielectric and air regions of the lattice as connected transmission lines with different characteristics impedances. Since the wavelength of the field is $2a$ at $k = \pi/a$, the length of the transmission line is $\lambda/2$ and therefore a full reflection should be appear i.e. the modes are standing waves with a wavelength of $2a$.

According to the EM variational theorem, low frequency modes concentrate their energy in high ϵ regions and high frequency modes accumulate their energy in low ϵ regions. With this in mind, we can see that the first band modes tend to accumulate their energy mostly in high ϵ regions and lower their frequency relatively. However, the second band forces most of its energy to shift in low ϵ regions since these two bands must be orthogonal to each other. Therefore the frequency of the second band becomes relatively higher than the first band (see Fig. 4.6). (The calculation of inner product of two modes are attached in appendix.)

With the knowledge of band gaps, we can observe that no electromagnetic modes are

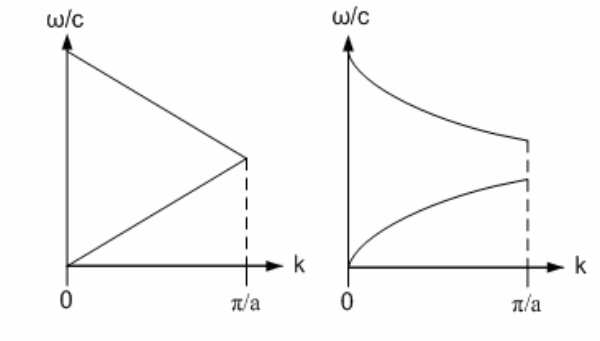

Figure 4.5: The first band structure belongs to uniform dielectric medium, the second one shows the band structure of a layered medium with a periodic dielectric contrast between layers.

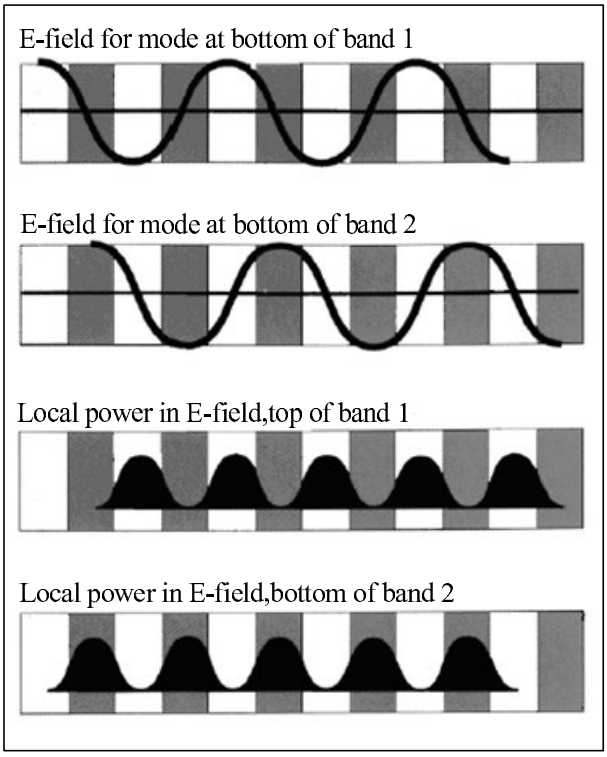

Figure 4.6: Schematic illustration of the modes associated with the lowest band gap of a one dimensional photonic crystal. The dark layers are low ϵ regions; the light layers are high dielectric.

allowed in the gap. But if this is the case, what happens when we send a wave with frequency in the photonic band gap onto the crystal? No purely real wave vector exists for any mode at that frequency so the wave amplitude decays exponentially in the crystal. When we say that there are no states in the photonic band gap, we mean that there are no extended states, instead the modes are evanescent. In order to understand this, we must examine the bands in the immediate vicinity of the gap. Revisiting Fig. 4.5, we try to approximate the second band near the gap by expanding $\omega_2(k)$ in powers of k about the zone edge $k = \pi/a$. Because of time reversal symmetry, $(\omega_2(k) = \omega_2(-k))$, the expansion cannot contain odd powers of k, so the lowest order becomes:

$$\Delta\omega = \omega_2(k) - \omega_2(\frac{\pi}{a}) = \alpha\left(k - \frac{\pi}{a}\right)^2 = \alpha(\Delta k)^2 \tag{4.27}$$

Now we can see where the complex wave vector originates. For frequency slightly higher than the top of the gap, $\Delta\omega > 0$. In that case, Δk is real and we are within the band 2. However for $\Delta\omega < 0$ (we are within the gap.), Δk is purely imaginary and the states decay exponentially [28].

4.2.4 Analysis of Two Dimensional Photonic Band Gap Materials via Plane Wave Method

A two dimensional photonic crystal is periodic along two of its axes (x and y axes in Fig. 4.7) and homogeneous along the third i.e. the dielectric function is $\epsilon(x, y) = \epsilon(x + a, y + a)$ where a is lattice constant. Some of the typical specimens of 2D crystals are square lattice of dielectric columns, square lattice of dielectric veins and triangular lattice. For certain values of the spacing of the columns or veins, the crystal can have a photonic band gap in the xy-plane. Inside the band gap, no extended states are permitted, and incident light is reflected. Although the multilayer film only reflects light at normal incidence, this two dimensional photonic crystal can reflect light incident from any direction in the plane.

Since the structure is uniform along the z-axis, according to symmetry properties, we can say that the fields must be independent of changes in z coordinate. Therefore the fields can be written of the form:

$$\vec{E} = E_x(x, y)\hat{x} + E_y(x, y)\hat{y} + E_z(x, y)\hat{z} \tag{4.28}$$

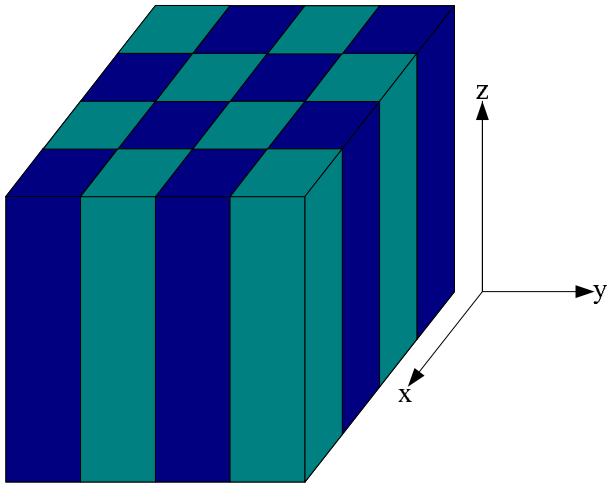

Figure 4.7: Simple example of two dimensional photonic crystal. Different colors correspond to materials with different dielectric constants.

$$\vec{H} = H_x(x,y)\hat{x} + H_y(x,y)\hat{y} + H_z(x,y)\hat{z} \tag{4.29}$$

When we substitute the above fields into the Maxwell's equations (**??**), we obtain two independent polarizations. If the electric field does not have a component on plane of incidence, the mode is denoted TE including the fields E_x, E_y and H_z. Similarly, if the electric field have on the plane of incidence, this mode is TM with fields H_x, H_y and E_z. Notice that finding E_x and H_z is sufficient to find all other field components at the same time.

TM polarization

$$\begin{aligned} \frac{\partial}{\partial z}E_z &= -j\omega\mu_0 H_x \\ \frac{\partial}{\partial x}E_z &= j\omega\mu_0 H_y \\ \frac{\partial}{\partial x}H_y - \frac{\partial}{\partial y}H_x &= j\omega\epsilon_0\epsilon_r(x,y)E_z \end{aligned} \tag{4.30}$$

TE polarization

$$\begin{aligned} \frac{\partial}{\partial y}H_z &= j\omega\epsilon_0\epsilon_r(x,y)E_x \\ \frac{\partial}{\partial x}H_z &= -j\omega\epsilon_0\epsilon_r(x,y)E_y \\ \frac{\partial}{\partial x}E_y - \frac{\partial}{\partial y}E_x &= -j\omega\mu_0 H_z \end{aligned} \tag{4.31}$$

From the first set (4.30), we obtain the following wave equation by eliminating H_x and H_y:

$$\frac{1}{\epsilon_r(x,y)}\left[\frac{\partial^2}{\partial x^2}+\frac{\partial^2}{\partial y^2}\right]E_z(x,y)=-\frac{\omega^2}{c^2}E_z(x,y) \tag{4.32}$$

Similarly, from the second set (4.31), the wave equation for TE polarization is obtained and notice that this equation is two dimensional version of the Hermitian master equation (4.6).

$$\left[\frac{\partial}{\partial x}\frac{1}{\epsilon_r(x,y)}\frac{\partial}{\partial x}+\frac{\partial}{\partial y}\frac{1}{\epsilon_r(x,y)}\frac{\partial}{\partial y}\right]H_z(x,y)=-\frac{\omega^2}{c^2}H_z(x,y) \tag{4.33}$$

4.2.5 Solution of Two Dimensional Master Equations by PWM

In order to solve (4.32) and (4.33), we must discretize the structure similar to the one dimensional case. Since the periodicity is along the *xy*-plane, the inverse dielectric function should be discretized in two dimensions by using two dimensional Fourier series expansion and field must be expressed by two dimensional Bloch-Floquet's theorem.

$$\frac{1}{\epsilon_r(x,y)}=\sum_m\sum_n C^{\epsilon}_{mn}e^{j\frac{2\pi m}{a}x}e^{j\frac{2\pi n}{a}y} \tag{4.34}$$

$$E_z(x,y)=\sum_m\sum_n C^{E}_{mn}e^{j\frac{2\pi m}{a}x}e^{j\frac{2\pi n}{a}y}e^{jk_xx}e^{jk_yy} \tag{4.35}$$

$$H_z(x,y)=\sum_m\sum_n C^{H}_{mn}e^{j\frac{2\pi m}{a}x}e^{j\frac{2\pi n}{a}y}e^{jk_xx}e^{jk_yy} \tag{4.36}$$

Similar to the one dimensional case, substituting (4.34) and (4.35) into (4.32) and rearranging the indices bring us to two dimensional eigenvalue relation for TM polarization as follows:

$$\sum_m\sum_n\left[\left(\frac{2\pi m}{a}+k_x\right)^2+\left(\frac{2\pi n}{a}+k_y\right)^2\right]C^{\epsilon}_{k-m,l-n}C^{E}_{m,n}=\frac{\omega^2}{c^2}C^{E}_{k,l} \tag{4.37}$$

Similarly, when we substitute (4.34) and (4.36) into (4.33) and rearrange the indices, we can obtain two dimensional eigenvalue relation for TE polarization.

$$\sum_m \sum_n \left[\left(\frac{2\pi m}{a} + k_x \right) \left(\frac{2\pi k}{a} + k_x \right) + \left(\frac{2\pi n}{a} + k_y \right) \left(\frac{2\pi l}{a} + k_y \right) \right] C^{\epsilon}_{k-m,l-n} C^{H}_{m,n} = \frac{\omega^2}{c^2} C^{H}_{k,l} \tag{4.38}$$

In order to put the eigenequations in to a matrix equation form, we should find the Fourier coefficients of the dielectric function according to the geometry of the lattice such that the square lattice with dielectric columns or square lattice with dielectric veins, triangular lattice etc. To find the dielectric coefficients, we must take the inverse Fourier transform of the inverse dielectric function by integrating in unit cell of the lattice such that:

$$C^{\epsilon}_{m,n} = \frac{1}{area[unitcell]} \int_x \int_y \frac{1}{\epsilon_r(x,y)} e^{-j\frac{2\pi m}{a}x} e^{-j\frac{2\pi n}{a}y} dxdy \tag{4.39}$$

We will see that we observe different band gap structures for each type of lattice geometry.

Square Lattice with Dielectric Columns

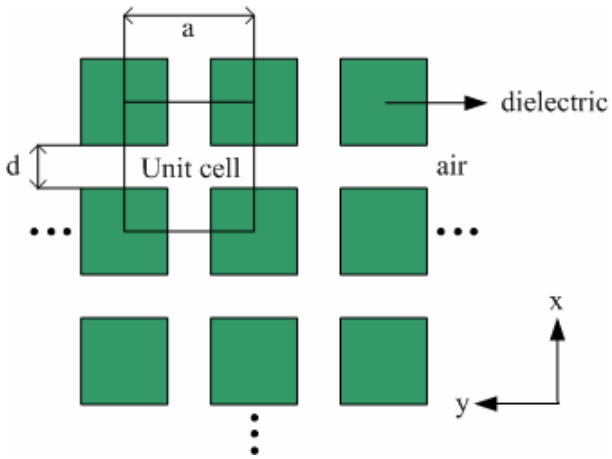

Figure 4.8: The geometry of dielectric columns in air.

We know from variational theorem, in order to minimize its energy, an electromagnetic field tends to concentrate its displacement field in the high ϵ regions which reduces the field frequency. On the other hand the solutions of our eigenvalue problem must be orthogonal to each other which means that for a fixed wave vector k two modes, belonging to different

bands, must be orthogonal in space. Photonic crystals with dielectric columns as in Fig. 4.8 has complete band gap for TM modes but not for the TE modes (see Fig. 4.10). Since for TM mode, electric and displacement fields are in the direction of uniform permittivity, the displacement field associated with lowest TM mode can be strongly concentrated in the dielectric regions while the second band of TM mode is accumulated in the air regions in order to keep orthogonal to the first mode. This separation causes a frequency difference between two bands so a band gap occurs for TM polarization. However for TE mode, the displacement field of both modes, belonging to first two bands, has significant amplitude in both air and dielectric region since displacement field extends in the xy-plane, so no frequency contrast appears.

The square lattice arrays have a square Brillouin zone, which is shown in Fig. 4.9. The irreducible Brillouin zone is the triangle in the upper right corner which is the blue region. Three special points Γ, X and M correspond to $k = 0$, $k = \frac{\pi}{a}\hat{x}$ and $k = \frac{\pi}{a}\hat{x} + \frac{\pi}{a}\hat{y}$ respectively.

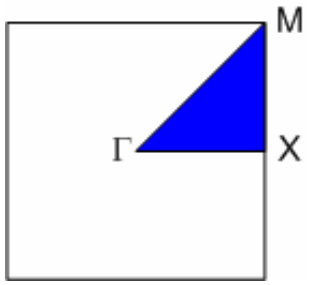

Figure 4.9: The Brillouin zone of the square lattice, centered at the origin Γ. The irreducible Brillouin zone is the blue triangular part of the zone. The special points are Γ, X and M, conventionally.

In Fig. 4.10 we can see the resulting band structure for both TE and TM modes. In order to simulate these band characteristics, we calculated the Fourier coefficients of the inverse dielectric functions according to (4.39) and specified dimensions of the unit cell in Fig. 4.8. Resulting coefficients are formulated as below:

$$C^{\epsilon}_{m,n} = \frac{d^2}{a^2}\left(\frac{1}{\epsilon} - 1\right) sinc\left(\frac{\pi dm}{a}\right) sinc\left(\frac{\pi dn}{a}\right) + \frac{1}{\epsilon}\delta_{mn} \tag{4.40}$$

In summary, the vector wave nature of the EM field is the main reason to band formation. The scalar D field of TM modes can be localized within the rods, but continuous field lines

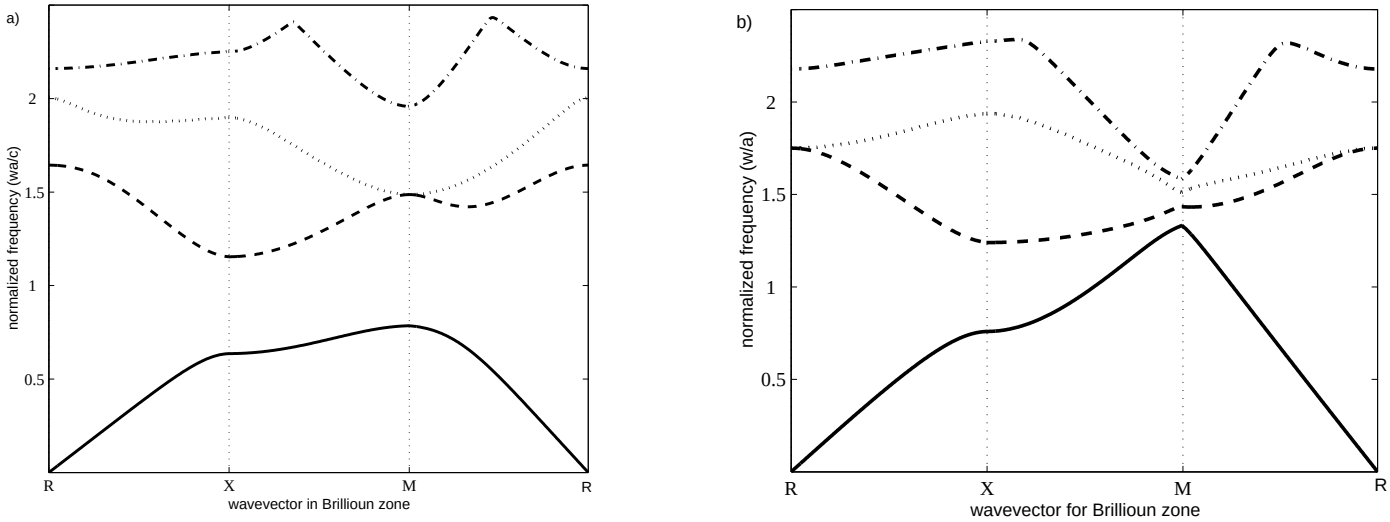

Figure 4.10: The photonic band structure for a square array of dielectric columns with air width $d = 0.7a$. The square columns ($\epsilon_r = 8$) are embedded in air ($\epsilon_r = 1$). *a*) TM mode with band gap. *b*) TE mode without a gap.

of TE modes are compelled to penetrate the air regions to connect neighboring rods. As a result consecutive TE modes can not exhibit a band gap.

Square lattice with dielectric veins

The structure is complementary to the square lattice with dielectric columns because it is a connected structure as seen in Fig. 4.11. The high ϵ regions form a continuous path in the *xy*-plane, instead of discrete spots. Therefore we see band gap in TE band structure but not for TM mode in this case.

For TM mode, we can see that both modes ,belonging to different bands, are confined within the high ϵ region. The fields of the dielectric band ($n = 1$) are confined to the dielectric crosses and vertical veins, whereas the fields of the air band ($n = 2$) are concentrated in the horizontal dielectric veins (Fig. 4.12). So two bands both manage to concentrate in high ϵ regions and therefore no sufficient jump in frequency occurs for a gap (Fig. 4.13). On the other hand, the TE band structure has a photonic band gap between the air and dielectric bands. In this case, the continuous field lines of the transverse D field can extend to neighboring lattice sites without leaving the high ϵ region. The veins provide high ϵ roads

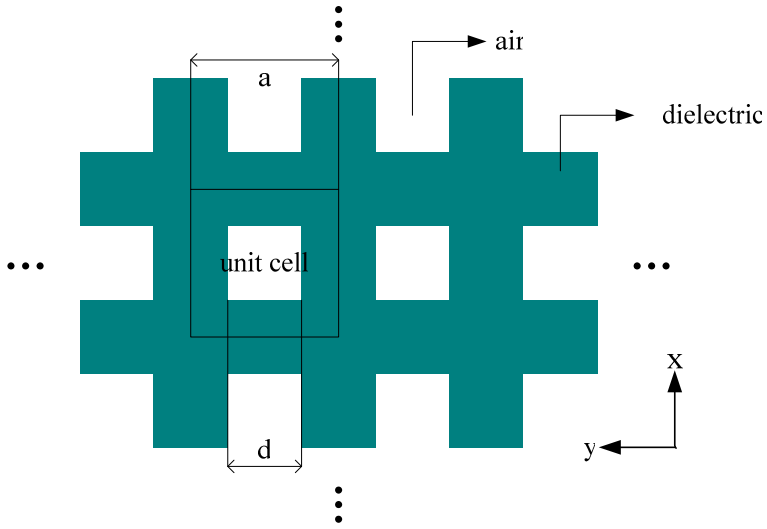

Figure 4.11: The geometry of dielectric veins in air.

for the fields to travel on and for $n = 1$ the field stay entirely on them. On the other hand, the D field of the next band is forced to enter the air regions in order to be orthogonal to the first band. So, some of the energy is thereby forced in to the air region which corresponds to a jump in frequency according to the variational theorem (Fig. 4.13).

In Fig. 4.13, we can see the resulting band structure for both TE and TM modes. In order to simulate these band characteristics, we calculated the Fourier coefficients of the inverse dielectric functions according to (4.39) and specified dimensions of the unit cell in Fig. 4.11. Resulting coefficients are formulated as below:

$$C^{\epsilon}_{m,n} = \frac{d^2}{a^2}\left(1 - \frac{1}{\epsilon}\right) sinc\left(\frac{\pi dm}{a}\right) sinc\left(\frac{\pi dn}{a}\right) + \frac{1}{\epsilon}\delta_{mn} \tag{4.41}$$

Triangular Lattice of Air Holes Embedded in a Dielectric Background

In the previous sections, we have seen that, two types of polarizations produce gaps in different geometries. In principle, TM band gaps occur in a lattice of isolated high ϵ regions, and TE band gaps are favored in a connected lattice. In order to create a band gap for both polarizations, we can construct crystals with high ϵ regions that are both practically isolated and linked by narrow veins. One of the examples of such a system is the triangular lattice of air columns as shown in Fig. 4.14.

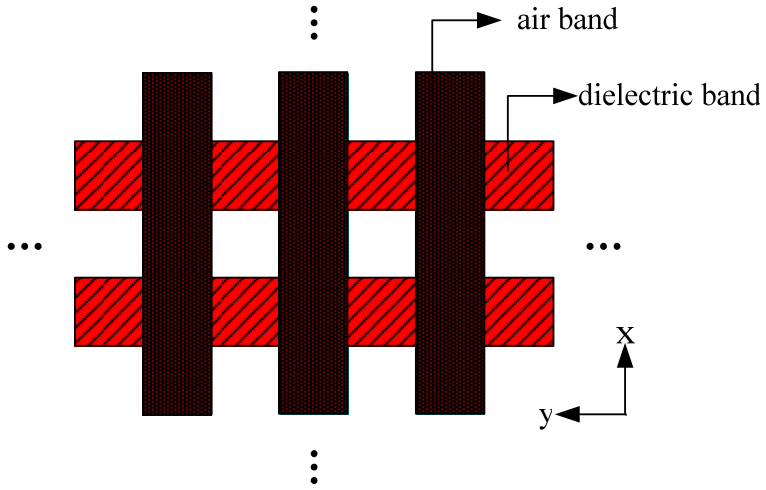

Figure 4.12: The arrangement of the electric fields of the TM mode within the dielectric veins. The first band (dielectric band) is localized vertically and the second band (air band) is horizontally along the xy plane, so both displacement field is confined in high ϵ region, which prevents frequency separation.

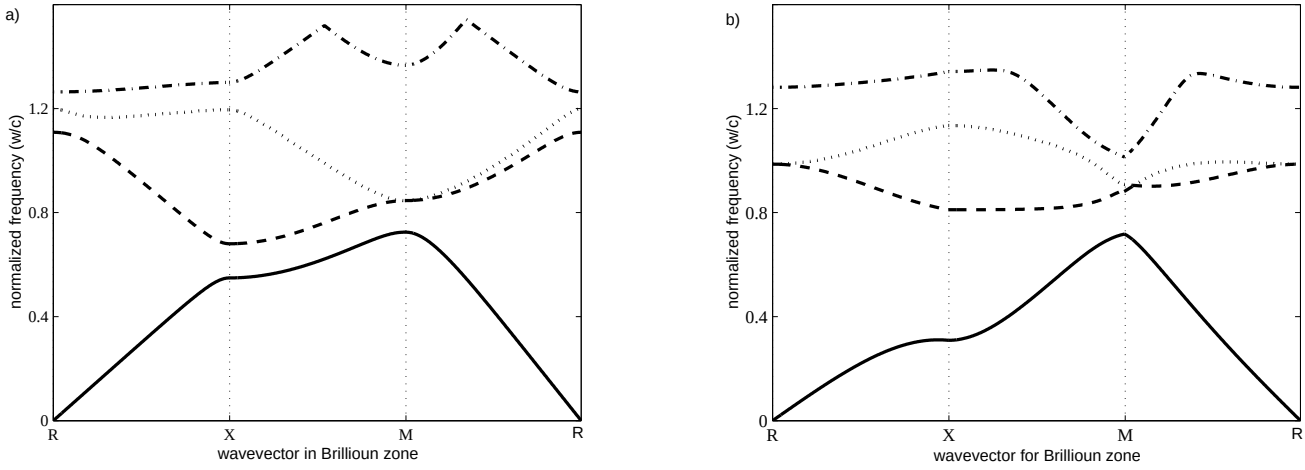

Figure 4.13: The photonic band structure for a square array of dielectric veins with air width $d = 0.6$. The square columns ($\epsilon_r = 19$) are embedded in air ($\epsilon_r = 1$). *a*) TM mode without band gap.*b*) TE mode with a gap.

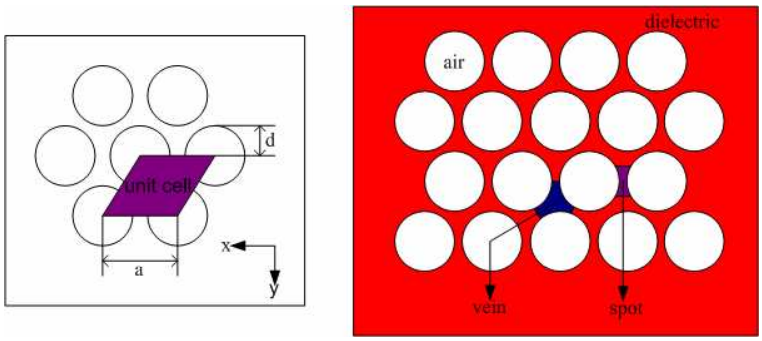

Figure 4.14: Two dimensional photonic crystals of air columns in a dielectric substrate. The air columns have radius d and dielectric constant $\epsilon_r = 1$. Spots are localized between the columns, veins are surrounded by three columns.

When we put a triangular lattice of low ϵ columns inside a medium with high ϵ and if the radius of the columns is large enough, the spots between columns look like localized regions of high ϵ material, which are connected to adjacent spots. Therefore we can see band gap for both TE and TM polarizations.

The triangular lattice arrays have a hexagonal Brillouin zone, which is shown in Fig. 4.15.The irreducible Brillouin zone is the triangle in the upper right corner which is the blue region. Three special points Γ, K and M correspond to $k = 0$, $k = \frac{\pi}{a}\hat{x} + \frac{\sqrt{3}\pi}{a}\hat{y}$ and $k = \frac{\sqrt{3}\pi}{a}\hat{y}$ respectively.

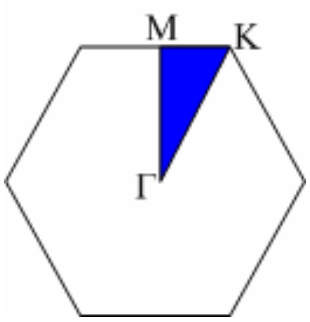

Figure 4.15: The Brillouin zone of the triangular lattice, centered at the origin Γ. The irreducible Brillouin zone is the blue triangular part of the zone. The special points are Γ, M and K, conventionally.

For this geometry, the primitive and reciprocal lattice vectors must be different from the previous cases and redefined since the unit cell is not square anymore. The primitive lattice

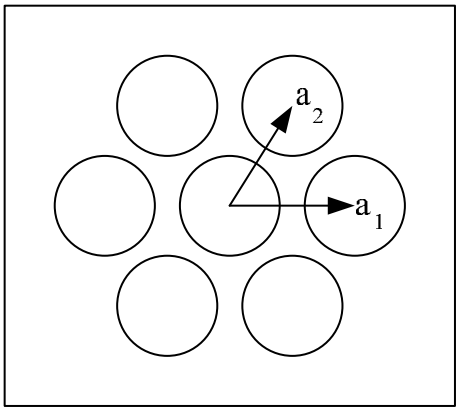

Figure 4.16: The location of the primitive lattice vectors according to the selected unit cell.

vectors are shown in Fig. 4.16.

$$\begin{aligned}\vec{a}_1 &= a\hat{x} \\ \vec{a}_2 &= a\left(\frac{1}{2}\hat{x} + \frac{\sqrt{3}}{2}\hat{y}\right) \\ \vec{b}_1 &= \frac{2\pi}{a}\left(\hat{x} - \frac{1}{\sqrt{3}}\hat{y}\right) \\ \vec{b}_2 &= \frac{2\pi}{a}\frac{2}{\sqrt{3}}\hat{y}\end{aligned} \tag{4.42}$$

For this case, two dimensional Fourier series of E, H fields and dielectric function is as follows:

$$\frac{1}{\epsilon(x,y)} = \sum_k \sum_l C_{kl}^{\epsilon} e^{j(k\vec{b}_1 + l\vec{b}_2)\cdot\vec{r}} \tag{4.43}$$

$$E_z, H_z(x,y) = \sum_k \sum_l C_{kl}^{E,H} e^{j(k\vec{b}_1 + l\vec{b}_2)\cdot\vec{r}} e^{j\vec{k}\cdot\vec{r}} \tag{4.44}$$

If we take the inner products over the exponentials as in (4.43) and (4.44), we get

$$\frac{1}{\epsilon(x,y)} = \sum_k \sum_l C_{kl}^{\epsilon} e^{j\frac{2\pi k}{a}x} e^{j\frac{2\pi(2l-k)}{a\sqrt{3}}y} \tag{4.45}$$

$$E_z(x,y) = \sum_k \sum_l C_{kl}^{E} e^{j\frac{2\pi k}{a}x} e^{j\frac{2\pi(2l-k)}{a\sqrt{3}}y} e^{jk_x x} e^{jk_y y} \tag{4.46}$$

$$H_z(x,y) = \sum_k \sum_l C_{kl}^H e^{j\frac{2\pi k}{a}x} e^{j\frac{2\pi(2l-k)}{a\sqrt{3}}y} e^{jk_x x} e^{jk_y y} \tag{4.47}$$

After substituting above series into (4.32) and (4.33), we get eigenequations below:

TM polarization:

$$\sum_k \sum_l C_{kl}^E C_{m-k,n-l}^{\epsilon} \left[\left(\frac{2\pi k}{a} + k_x \right)^2 + \left(\frac{2\pi(2l-k)}{a\sqrt{3}} + k_y \right)^2 \right] = \frac{\omega^2}{c^2} C_{mn}^E \tag{4.48}$$

$$\sum_k \sum_l C_{kl}^H C_{m-k,n-l}^{\epsilon} \left[\left(\frac{2\pi k}{a} + k_x \right) \left(\frac{2\pi m}{a} + k_x \right) + \left(\frac{2\pi(2l-k)}{a\sqrt{3}} + k_y \right) \cdot \left(\frac{2\pi(2n-m)}{a\sqrt{3}} + k_y \right) \right] = \frac{\omega^2}{c^2} C_{mn}^H \tag{4.49}$$

When we solve these equations, band gap occurs for both polarizations. This is shown in Fig. 4.17.

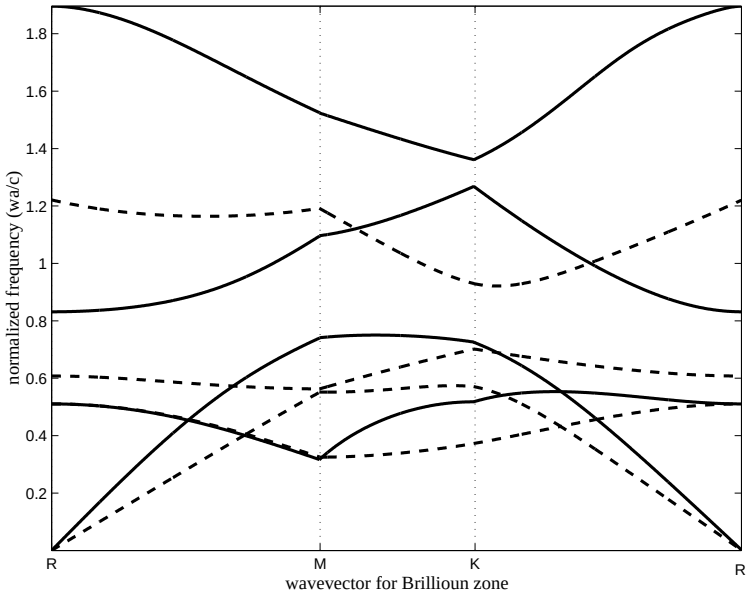

Figure 4.17: The photonic band structure for the modes of a triangular array of air columns (d=0.55) embedded in a dielectric substrate (ϵ=10). The solid lines represent TE bands and the dashed lines represent TM bands.

Fig. 4.18 shows a limiting case of the triangular lattice in order to understand the existence of both connectivity and isolation. As you see from the figure, dielectric regions

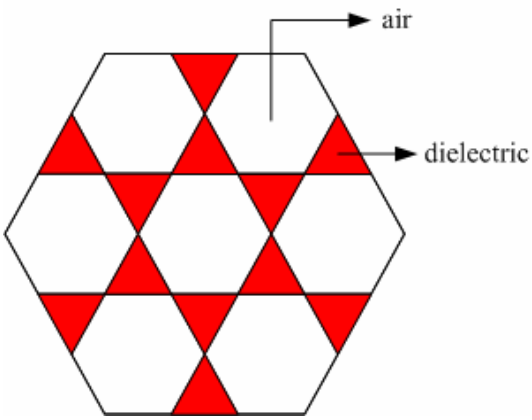

Figure 4.18: The hexagonal (extreme) case of the triangular lattice in order to understand connectivity and isolation concept. As an extreme case, dielectric columns are both isolated in practice and connected in one point at the same time.

are connected to each other at one point therefore they can be thought that they are connected but also they are still isolated as dielectric columns practically.

So far, one and two dimensional photonic crystals, which are assumed to fill the entire space, are reviewed by describing the analysis approach, namely plane wave method. In the following sections, a novel analysis method is presented and plane wave method is used to confirm the accuracy of this new approach and differences are validated.

4.2.6 Analysis of Finite One Dimensional Photonic Band Gap Materials via GPOF method

In the previous section, one-dimensional photonic crystals have been studied using the plane wave method, for which the periodic structure is assumed to fill the entire space. However, for a realistic case of a one-dimensional photonic crystal with a finite number of layers, the plane wave method is not suitable, and to the best of our knowledge, there is no efficient method that would provide the dispersion diagram ($\omega - k$ diagram). In this section, a novel method, based on the generalized reflection coefficient at the air-PhC interface and the generalized pencil of function method [29], is proposed, developed and validated. In addition to providing the dispersion characteristics of the structure, it also provides the equivalent homogenization parameters of the periodic structure. Therefore, the proposed method does not only help to understand the propagation of light in a finite extend photonic crystal, but also helps to find its homogenous equivalent.

It has been reviewed that, in the plane wave method, all possible solutions are obtained as the sum of plane waves by scanning the wave vector over the entire irreducible Brillouin zone, whereas the proposed method makes use of the reflection data for an incident plane wave at a specific frequency and obtain its corresponding wave vector information. In other words, while frequencies are the solutions with the knowledge of wave vectors in the plane wave method, wave vectors are the outputs of the proposed method for a given frequency of the incident wave. In this approach, for some frequencies, the wave vectors turn out to be purely imaginary, which is the indication of non-propagating waves (i.e., evanescent waves) at these frequencies. The frequency band corresponding to non-propagating region is also referred to as the band gap of the structure.

Method of finding band structure and homogenization parameters:

A one-dimensional, finite photonic crystal in free-space, as shown in Fig. 4.19, is considered to demonstrate the steps of the proposed method. The first step of the method is to find the generalized reflection coefficients due to a normal incident plane wave for different number of unit cells, following the procedure outlined in Chapter 2. Then, the photonic crystal is assumed to be replaced by a material slab in free-space, i.e., a three-layer medium, whose generalized reflection coefficients are made to be equivalent to those of the photonic crystal. The generalized reflection coefficient at the air-dielectric interface of this three

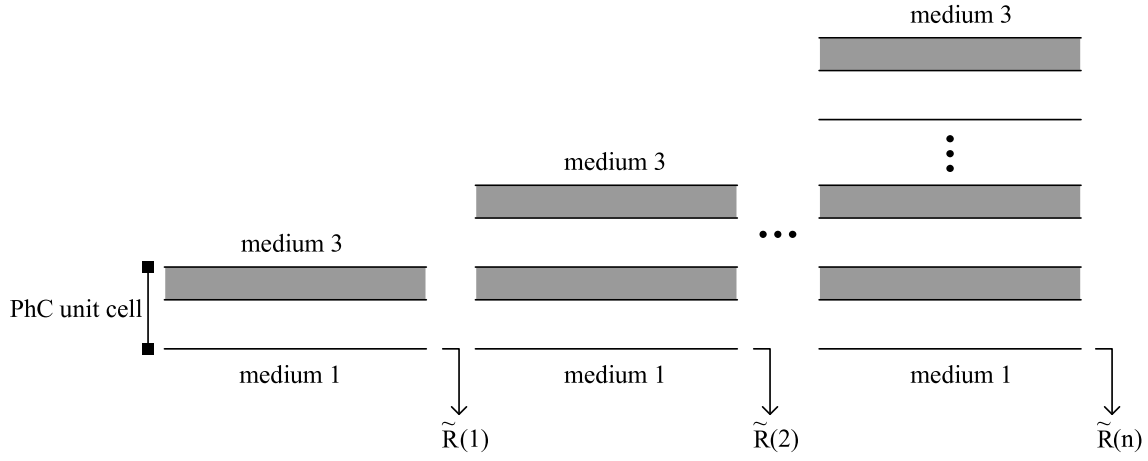

Figure 4.19: Reflection coefficient collection procedure. $\widetilde{R}(n)$ are thickness dependent reflection coefficients. Incident wave is sent from Medium 1.

layered medium is given as

$$\begin{aligned}\widetilde{R}_{1,2} &= R_{1,2} + \frac{T_{1,2}T_{2,1}R_{2,3}e^{-jk_2 2d}}{1 - R_{2,3}R_{2,1}e^{-jk_2 2d}} \\ &= R_{1,2} + T_{1,2}T_{2,1}R_{2,3}e^{-jk_2 2d} + T_{1,2}T_{2,1}R_{2,1}R_{2,3}^2 e^{-jk_2 4d} + ... \end{aligned} \tag{4.50}$$

where k_2 is the wave number and d is the thickness of medium-2, and $R_{i,j}$ and $T_{i,j}$ are the Fresnel reflection and transmission coefficients defined at the interface between medium-i and medium-j. It should be noted that medium-2 is composed of number of unit cells of photonic crystal positioned in free-space, and that (4.50) is valid for both TE and TM modes, except for the Fresnel refection coefficient $R_{1,2}$. The Fresnel reflection coefficients for TE and TM waves for normal incidence are rewritten as

$$R_{1,2}^{TE} = \frac{\mu_2 k_1 - \mu_1 k_2}{\mu_2 k_1 + \mu_1 k_2} \tag{4.51}$$

$$R_{1,2}^{TM} = \frac{\epsilon_2 k_1 - \epsilon_1 k_2}{\epsilon_2 k_1 + \epsilon_1 k_2} \tag{4.52}$$

Since the generalized reflection formula for a three-layer medium can be written in terms of the exponential functions of the thickness of the homogeneous slab,(4.50), if the generalized reflection coefficient from a finite photonic crystal in free-space can be written in terms of the exponentials of the thickness, one can easily obtain a relation between the three-layer structure and the photonic crystal. To do so, the generalized reflection coefficients are calculated at the air-photonic crystal interface for different number of unit cells in medium-2, that is, for different thicknesses of the crystal, as illustrated in Fig. 4.19. If there is an equivalent homogenous material for the photonic crystal, then the reflection coefficient data collected for different thicknesses would be approximated in terms of complex exponentials by the GPOF method. The result of the GPOF method would be in the following form:

$$A_0 + A_1 e^{B_1} + A_2 e^{B_2} + ... \tag{4.53}$$

where the direct term A_0 and the exponent of the largest magnitude must be equal to the Fresnel reflection term and $-jk_2 2d$ in (4.50), respectively. Hence, the wave number of medium-2, k_2, is obtained as

$$k_2 = \frac{jB_{max}}{2a} \tag{4.54}$$

where B_{max} is the exponent of the largest magnitude, and a is the length of the unit cell, which is also referred to as the lattice constant of the photonic crystal. Once the equivalent

wave number of medium-2, k_2, is obtained for a given frequency, the same procedure is repeated until enough data are gathered to form the dispersion diagram. In addition, the electric and magnetic parameters of the equivalent medium can be obtained simply from the Fresnel reflection coefficients using the equivalent wave number. This procedure can be considered as the homogenization of the photonic crystal, with the homogenization parameters μ_2 and ϵ_2

$$\mu_{r2} = \frac{(1 + R_{1,2})k_2}{(1 - R_{1,2})k_1} \tag{4.55}$$

$$\epsilon_{r2} = \left[\frac{k_2 c_0}{2\pi f}\right]^2 / \mu_{r2} \tag{4.56}$$

where $\mu_{r1} = 1$, k_1 $(= 2\pi f/c_0)$ is the wave number of media-1 and -3, f denotes the frequency of incident wave, and c_0 is the speed of light in vacuum. Although the procedure here is provided and demonstrated for a normal incident TE wave, it is the same for a TM wave. However, for oblique incidence, the calculations need to be performed in the direction of propagation, whose details will be studied in the next section.

Results and Discussions

The first two bands of the photonic crystal, whose parameters are given in Fig. 4.4, are obtained following the procedure described above, and provided in Fig. 4.20. It should be noted that the wave numbers obtained may not correspond to the reduced Brillouin zone for given frequencies, but, due to the periodicity of the exponential terms, they should satisfy the following relation:

$$e^{-jk_2 2d} = e^{-j(k_2 d \pm n\pi)2} = e^{-jk_2 2d} \underbrace{e^{\pm jn2\pi}}_{1}$$

where n is an integer. Therefore, using the above relation, one can easily find the wave number in the irreducible Brillouin zone, by shifting the one obtained directly from the GPOF method. As a result, the proposed approach based on the GPOF method can predict the dispersion characteristics of a finite photonic crystal very accurately, as shown in Fig. 4.20. It should be stressed here one more time that the plane wave method can not be used to find the dispersion diagram of a finite structure.

In order to confirm that the wave number obtained from the proposed method actually corresponds to the homogenous equivalent of the photonic crystal at a given frequency, the

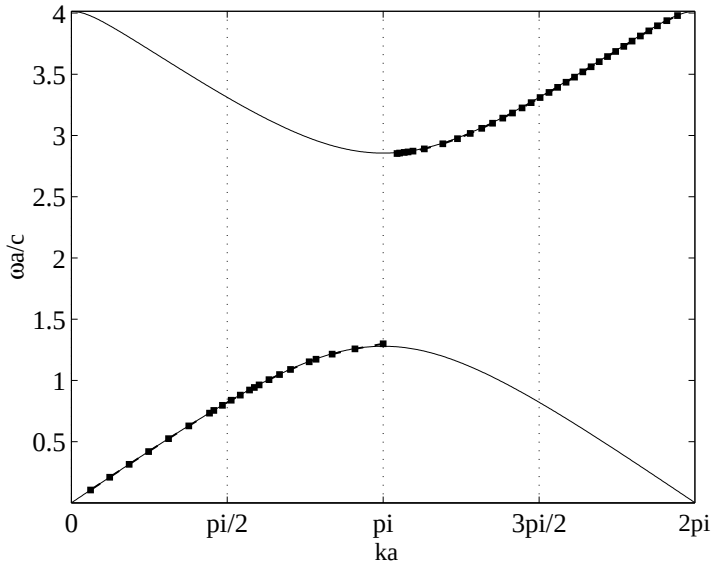

Figure 4.20: *Solid Line*: First two bands of a multilayer film with constant a and alternating layers of different widths. The width of the $\epsilon_r = 13$ layer is $0.2a$,and the width of the $\epsilon_r = 1$ layer is $0.8a$. Band structure is found by PWM. *Pointed Data*: Band structure of the same periodicity with 102 layer photonic crystal found by GPOF approach.

exponents of the higher order terms obtained from the GPOF method, (4.53), are checked if the wave numbers calculated are the same as the one obtained from the first exponential term above. This concern has been alleviated by calculating the wave number from the exponents of the third and fourth terms in (4.50), that is, from $-jk_2 4a$ and $-jk_2 6a$, and the results are provided in Fig. 4.21. Note that the wave numbers obtained from the third and fourth terms need to be shifted by $\pi/2$ and $\pi/3$, respectively, to bring the values into the irreducible Brillouin zone, as these terms have the periodicity of $\pi/2$ and $\pi/3$, respectively. Once shifted, the results obtained from the first three exponents agree quite well, implying that the photonic crystal can be homogenized and that the wave normally incident to this structure at the given frequency will reflect as it would reflect from its homogenous equivalent.

For the method proposed in this thesis, the primary data necessary for the application of the GPOF method is the generalized reflection coefficient defined at the interface between the air and the crystal. Therefore, it would be good to see the magnitude of the reflection

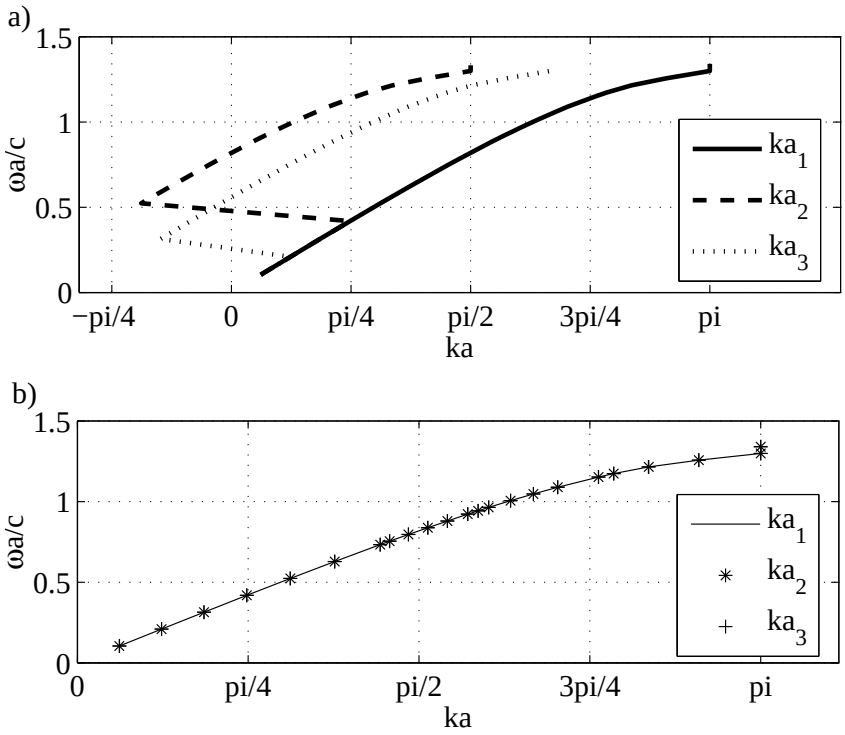

Figure 4.21: *a*) Three k values obtained from the first three exponentials of the GPOF method without shift. *b*) ka_2 and ka_3 values of the first figure are shifted by $\pi/2$ and $\pi/3$, respectively. Solid line represents the band calculated from the regular GPOF approach.

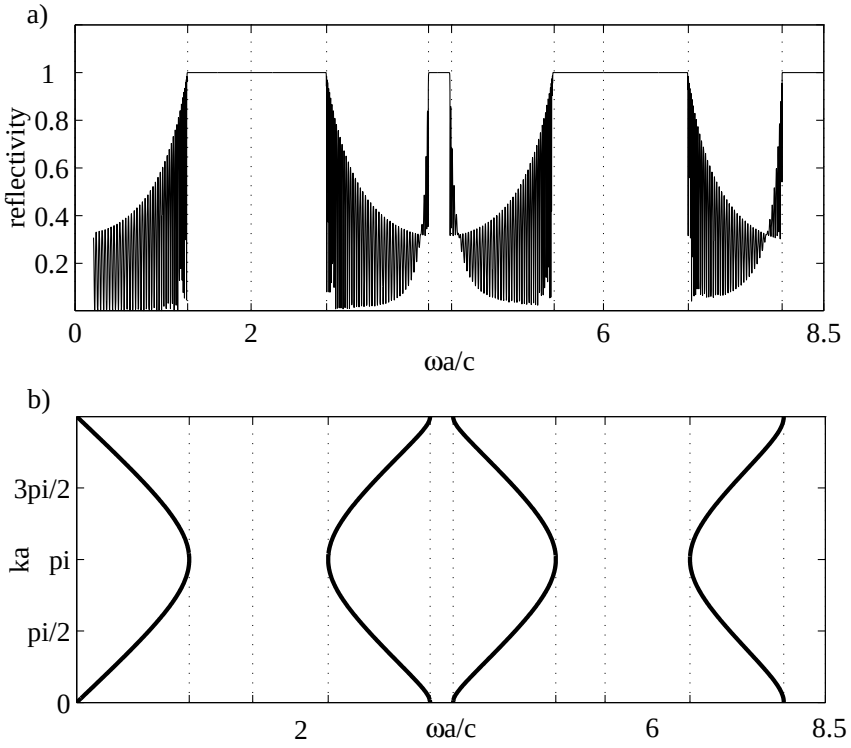

Figure 4.22: *a*) The magnitude of the reflection coefficient vs frequency relation of an 102 layer photonic crystal in air with a lattice constant $a = 200$ nm. The width of the dielectric $\epsilon = 13$ is $0.2a = 40$ nm, and the width of the $\epsilon = 1$ layer is $0.8a = 160$ nm. *b*) The photonic band structure of a multilayer film found by PWM with lattice constant a and alternating layers of different widths. The width of the $\epsilon = 13$ layer is $0.2a$, and the width of the $\epsilon = 1$ layer is $0.8a$.

coefficient over a frequency band that covers both the band gap and the band pass regions. This would also provide information how a finite photonic crystal behaves as compared to its infinite (ideal) extension. As it is observed from Fig. 4.22, the frequency band for the total reflection from a finite photonic crystal agrees well with the band gap of an ideal infinite crystal composed of the same materials. The first plot of Fig. 4.22 shows the magnitude of the generalized reflection coefficient over a frequency band at the first interface of the photonic crystal, and the second one is the band structure of the same photonic crystal.

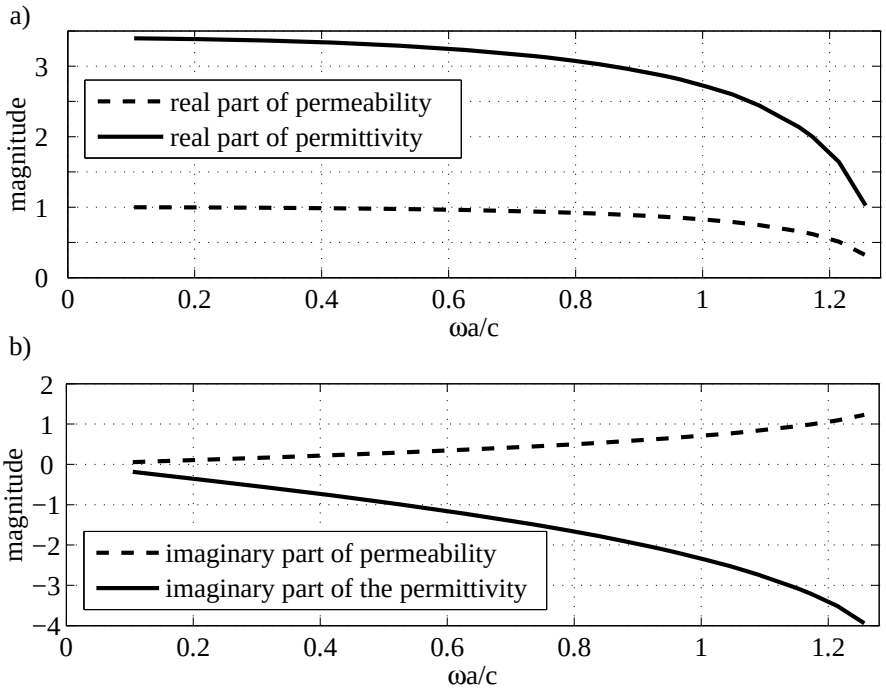

Figure 4.23: *a*) The real part of the permittivity and permeability of the homogeneous equivalence of the 102 layered photonic crystal for the first transmission band. *b*) The imaginary part of the permittivity and permeability of the homogeneous equivalence of the 102 layered photonic crystal for the first transmission band.

Once the method is implemented to find the dispersion diagram, and validated with the comparison to the results obtained from the plane wave method, it can now be extended to find the homogenization parameters of such finite crystals. From the above discussions, it

was obvious that the crystal has behaved as a homogenous medium for the incident wave over a frequency band. Therefore, with the knowledge of the equivalent wave number for the crystal structure, the real and imaginary parts of the effective permittivity and permeability are obtained, following the procedure detailed in the previous section, and provided in Fig. 4.23. As an observation, the real parts of both permittivity and permeability decrease while approaching to the photonic band gap, and the magnitudes of their imaginary parts increases. Perhaps more subtle point to discuss is the imaginary part of the equivalent permeability, which assumes positive values over the entire band of the homogenization. If the time convention is remembered one more time as $e^{j\omega t}$, the imaginary parts of the permittivity and permeability of a realistic passive material has to be negative. Therefore, since the equivalent parameters have been obtained based on only the reflection data at the incidence plane of the photonic crystal, it would be necessary and instructive to compare the field distributions in the photonic crystal and the homogenized medium. Only then, it would be accurate to refer the homogenized medium to as the equivalent of the crystal structure.

Fig. 4.24 represents two different field distributions inside the crystal and its homogeneous equivalent for two operating frequency. It is found that, the distribution of the fields inside the crystal and its homogeneous model are in agreement for the incident waves propagating with frequencies away from the gap frequencies. As we send plane waves which have frequency near the gap, this agreement fails. This is because of the fact that, the real propagations cease to exist and only evanescent fields start to be supported inside the crystal. However, since an effective permittivity and permeability are defined by the approach, there must be a propagation in the homogeneous equivalent inevitably due to the normal incidence. In other words, a homogeneous medium can not support only the evanescent fields inside, while a plane wave enters the medium normally. Hence we conclude that, the field distributions inside the crystal agree with ones inside the homogenized medium for the band frequencies which are not close to band gap frequency. Therefore, the positive permeability can be explicable for modeling purposes.

Oblique incidence

While the method was being introduced in the previous section, the derivation of the dispersion diagram and the equivalent parameters for the oblique incidence was briefly men-

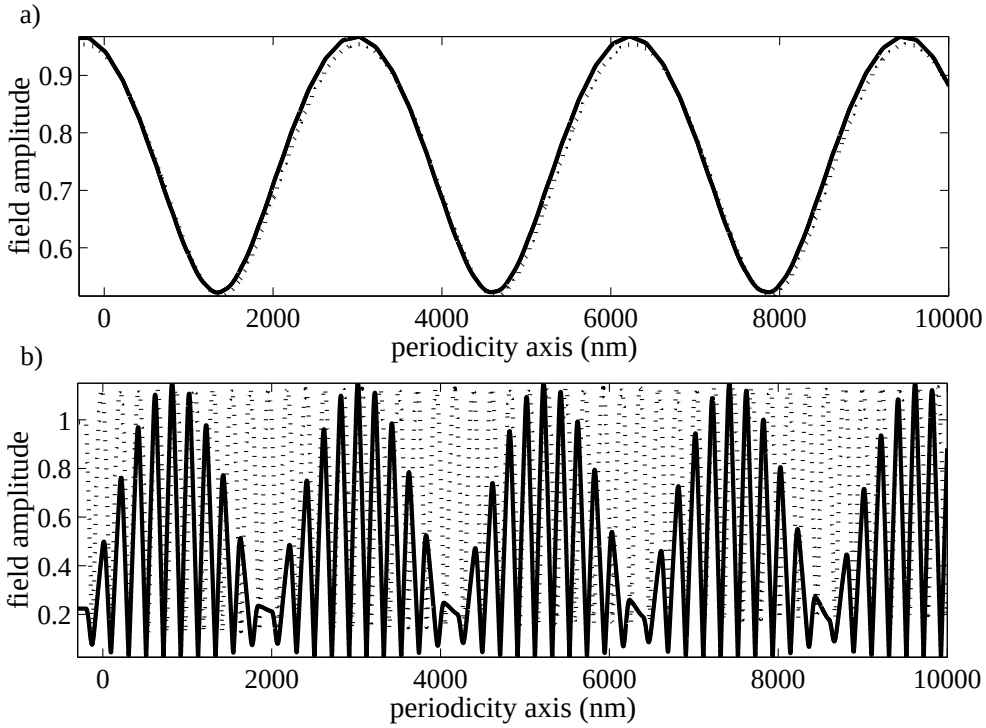

Figure 4.24: Pointed lines represent the fields of the homogeneous equivalence and solid line is the fields of the crystal itself. Photonic crystal is composed of 51 lattices with $200nm$ length. For each lattice, dielectric layer is $40nm$ and air is $160nm$. *a*) The field representations in 25 THz. *b*) The field representations in 300 THz. This photonic crystal has a band gap beginning at 310 THz.

tioned and referred to this section to be detailed. Since the method proposed in this thesis is based on the collected reflection data for a set of thicknesses of the periodic structure, it can still be applied for the case of oblique incidence provided that the wave number over the exponents are replaced by the propagation constant along the direction of the periodicity, k_z in this case. In other words, the only difference between the analysis of the normal and oblique incidences is the choice of the wave vector taken into account: for oblique incident wave, all formulations including the wave number of the medium, as stated k in the previous sections, must be replaced by k_z. Remember that the other component of the wave vector (k_x or k_y according to coordinate selection) must be the same in each layer due to the phase matching condition. The steps of the modified method is basically as follows: For TE mode, the generalized reflection coefficient can be written as

$$\widetilde{R}^{te}_{1,2} = R^{te}_{1,2} + T^{te}_{1,2}T^{te}_{2,1}R^{te}_{2,3}e^{-jk^{te}_{z2}2d} + T^{te}_{1,2}T^{te}_{2,1}R^{te}_{2,1}{R^{te}_{2,3}}^{2}e^{-jk^{te}_{z2}4d} + ... \tag{4.57}$$

and the approximation by the GPOF method will be in the following form:

$$A^{te}_0 + A^{te}_1 e^{B^{te}_1} + A^{te}_2 e^{B^{te}_2} + ... \tag{4.58}$$

By comparing (4.57) and (4.58), one can easily obtain the equivalent propagation constant and the permeability in medium-2 (periodic structure) as

$$k^{te}_{z2} = \frac{jB^{te}_{max}}{2a} \tag{4.59}$$

$$\mu_{r2} = \frac{(1 + A^{te}_0)k^{te}_{z2}}{(1 - A^{te}_0)k_{z1}} \tag{4.60}$$

Similarly, using an incident TM wave, ϵ_{r2} is obtained as

$$k^{tm}_{z2} = \frac{jB^{tm}_{max}}{2a} \tag{4.61}$$

$$\epsilon_{r2} = \frac{(1 + A^{tm}_0)k^{te}_{z2}}{(1 - A^{tm}_0)k_{z1}} \tag{4.62}$$

In Fig. 4.25 the first transfer band can be seen for normal incidence, 30^o and 60^o incidences for both TE and TM waves. The angle of incidence for TE waves does not cause a significant deviation to band gap frequency compared to TM mode case. It can be seen in the first part of Fig. 4.25. On the other hand, for TM mode, the band gap begins at a higher frequency as seen in the second part of the figure. As we constitute the band structure of

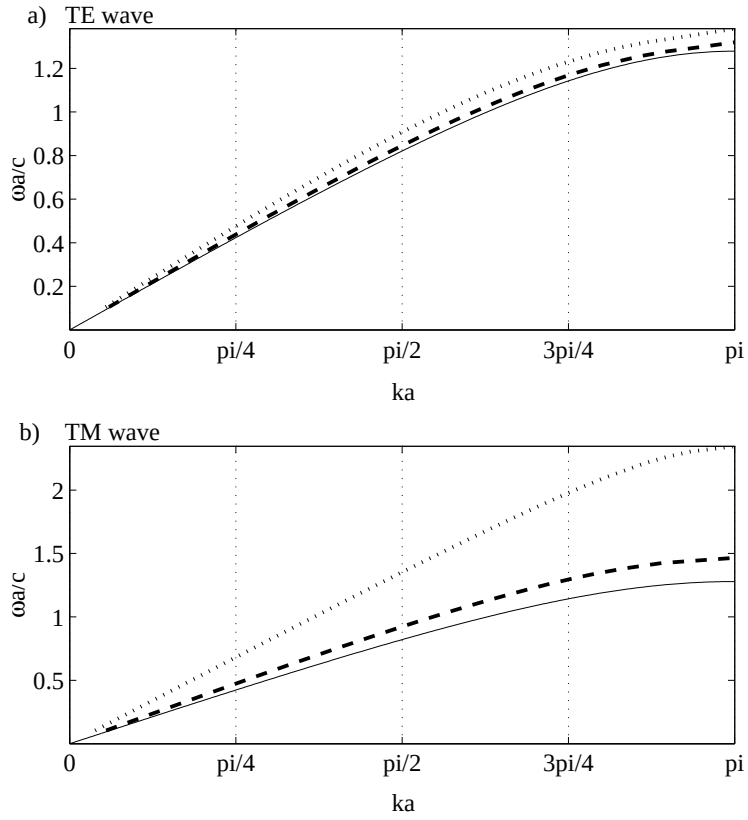

Figure 4.25: The first transmission band of a 102 layer photonic crystal in air with a lattice constant $a = 200$ nm. The width of the dielectric $\epsilon = 13$ is $0.2a = 40$ nm, and the width of the $\epsilon = 1$ layer is $0.8a = 160$ nm. *a*) The band for TE waves. *b*) The band for TM waves. Solid line represent the band for normal incidence, the dashed and pointed line show the band of 30^o and 60^o of incidences, respectively.

the photonic crystal for oblique incidence, their effective permeability and permittivity deviations according to angle of incidences can also be analyzed by the same principles. Fig. 4.26 and Fig. 4.27 represent these relations.

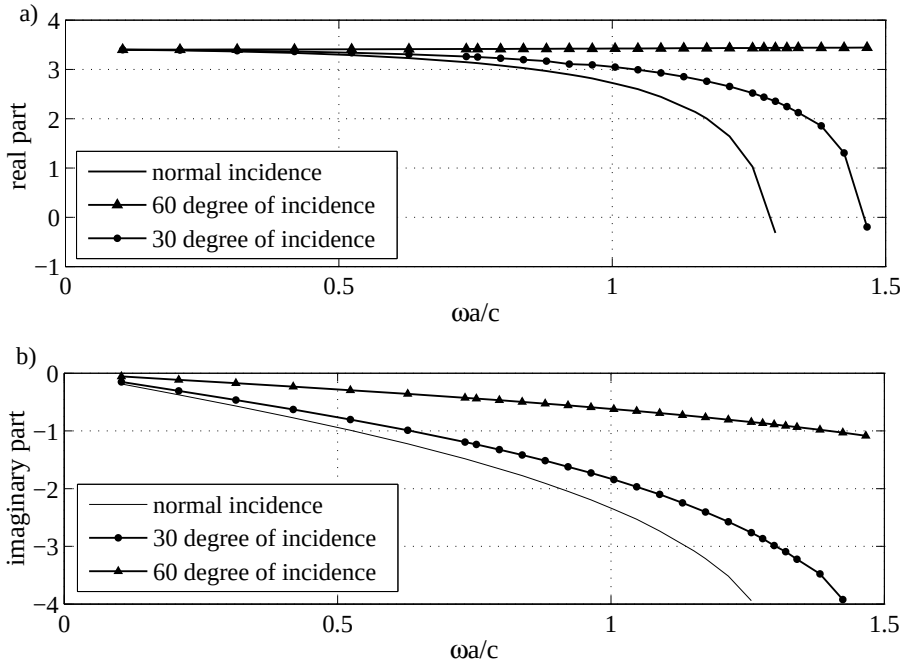

Figure 4.26: The effective relative permittivity of a finite photonic crystal with a lattice constant $a = 200$ nm. The width of the dielectric $\epsilon_r = 13$ is $0.2a = 40$ nm, and the width of the $\epsilon_r = 1$ layer is $0.8a = 160$ nm. *a*) The real part of the relative permittivity. *b*) The imaginary part of the relative permittivity. Solid line is for normal incidence, the dashed and pointed lines show the permittivity for 30^o and 60^o of incidences, respectively.

To sum up, one of the advantages of the method proposed in this thesis is its ability to analyze the photonic crystals for also oblique incident waves. Since the plane wave method assumes an infinite extend of structure, the oblique propagation can not be considered. By our new approach, we can analyze and investigate the changes on band gap and effective permittivity and permeability of a crystal for any incident angle.

In this chapter our main goal was to fully understand nature of the photonic crystal including its physical system, periodicity, gap phenomenon and analysis. In order to achieve this, we tried to explain the nature of one and two dimensional photonic crystals via plane

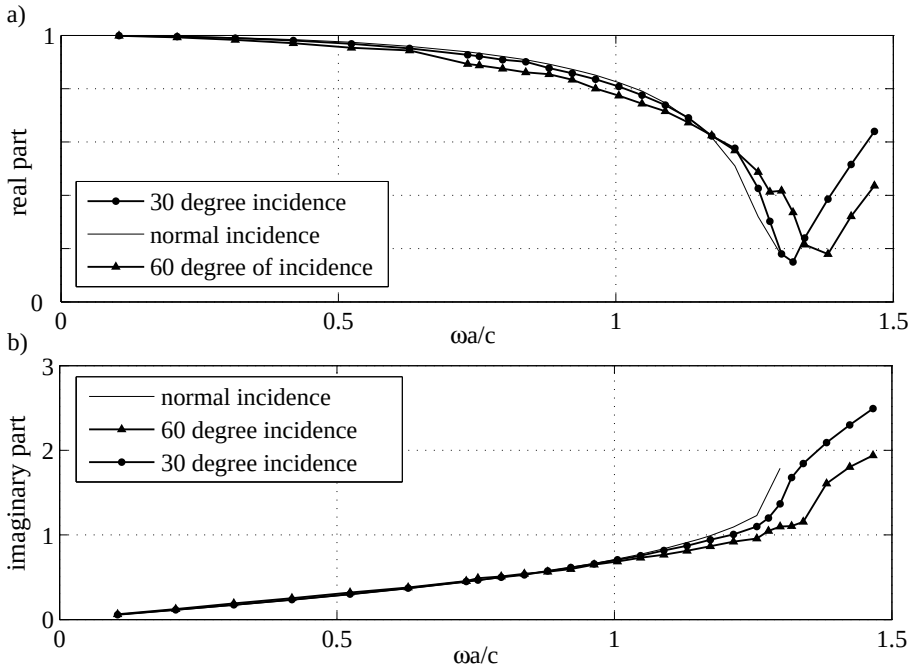

Figure 4.27: The effective relative permeability of a finite photonic crystal with a lattice constant $a = 200$ nm. The width of the dielectric $\epsilon_r = 13$ is $0.2a = 40$ nm, and the width of the $\epsilon_r = 1$ layer is $0.8a = 160$ nm. *a*) The real part of the relative permeability. *b*) The imaginary part of the relative permeability. Solid line is for normal incidence, the dashed and pointed lines show the permeability for 30^o and 60^o of incidences, respectively.

expansion method. Then we proposed an alternative method namely GPOF approach for one dimensional photonic crystals. This new approach gave us an opportunity to get the dispersion characteristics of photonic crystals which do not have an infinite periodicity, on the contrary, have limited alternating layers. In addition, with this approach we could find their homogeneous models.

In principle, this approach can also be modified to obtain the dispersion scheme of two and three dimensional photonic crystals as well. The $\omega - k$ diagram of higher dimensional photonic crystals can be obtained via this method by just stacking the two or three dimensional lattices this time and calculating the resulting reflections from these periodic structures. If we fit these set of data to the reflection expression of their homogeneous equivalent, we can obtain the dispersion characteristics and homogeneous models for these more complicated geometries.

4.3 Appendix

4.3.1 Inner Product and Orthogonality

We define the inner product of two vector fields $\vec{F}(r)$ and $\vec{G}(r)$ as

$$(\vec{F}, \vec{G}) = \int dr \vec{F}^*(r) \cdot \vec{G}(r) \tag{4.63}$$

Note that,$(\vec{F}, \vec{G}) = (\vec{G}, \vec{F})^*$ for any $\vec{F}(r)$ and $\vec{G}(r)$. Also note that $(\vec{F}, \vec{F})$ is always real even if $\vec{F}$ itself is complex.

In order to understand the orthogonality concept, we can simply examine two real one-dimensional functions $f(x)$ and $g(x)$. The orthogonality of these functions means that

$$(f, g) = \int f(x)g(x)dx = 0 \tag{4.64}$$

Basically, the product $f.g$ must be negative as much as it is positive over the interval of interest, so that the net integral vanishes. For instance, the set of functions $f_n(x) = \sin(n\pi x)$ are all orthogonal in the interval between $x = [0, 1]$. Note that all have different number of nodes, where $f_n(x) = 0$. The product of any two different f_n is positive as often as it is negative in order to make the inner product 0.

In our case we consider more complicated functions which are higher dimensional vector fields. In this case however the fact that orthogonal modes of different frequency have different number of nodes in space still holds. Generally, a harmonic mode has more nodes than lower-frequency modes.

4.3.2 The Eigenvector $\nabla \times \left[\frac{1}{\epsilon(\vec{r})}\nabla \bullet\right]$ *is Hermitian*

An operator Θ is Hermitian if $(\vec{F}, \Theta\vec{G}) = (\Theta\vec{F}, \vec{G})$ for any vector fields. In order to show that Θ is Hermitian, we perform integration by parts twice:

$$\begin{aligned}(\vec{F}, \Theta\vec{G}) &= \int dr\vec{F}^* \cdot \left\{\nabla \times \left[\frac{1}{\epsilon}\nabla \times \vec{G}\right]\right\} \\ &= \int dr(\nabla \times \vec{F})^* \cdot \frac{1}{\epsilon}\nabla \times \vec{G} \\ &= \int dr \cdot \left\{\nabla \times \left[\frac{1}{\epsilon}\nabla \times \vec{F}\right]\right\}^* \cdot \vec{G} \\ &= (\Theta\vec{F}, \vec{G}) \end{aligned} \tag{4.65}$$

4.3.3 Hermitian Properties

1. The Hermitian operator Θ must have real eigenvalues:

   Knowing that Hermiticity dictates $(\vec{H}, \Theta\vec{H}) = (\Theta\vec{H}, \vec{H})$ where the inner product is defined by $(\vec{H}, \Xi\vec{H}) = (\Xi\vec{H}, \vec{H})^*$ for any operator Ξ, we can show that

   $$(\vec{H}, \Theta\vec{H})^* = \left(\frac{\omega^2}{c^2}\right)^* (\vec{H}, \vec{H}) = (\Theta\vec{H}, \vec{H}) = \left(\frac{\omega^2}{c^2}\right)(\vec{H}, \vec{H}) \tag{4.66}$$

   Then

   $$\left(\frac{\omega^2}{c^2}\right)^* = \left(\frac{\omega^2}{c^2}\right) \tag{4.67}$$

   It follows that $\omega^2 = (\omega^2)^*$ then ω^2 is real.

2. All eigenvalues of an Hermitian equation must be positive:

   If we set $F = G$ as H in the second line of the equation 4.65, we obtain

   $$(\vec{H}, \vec{H})\left(\frac{\omega^2}{c^2}\right) = (\vec{H}, \Theta\vec{H}) = \int dr\frac{1}{\epsilon}\left|\nabla \times \vec{H}\right|^2 \tag{4.68}$$

Since $\epsilon(r) > 0$, the integrand on the right hand side is everywhere positive. Therefore all eigenvalues must be positive.

3. The Hermiticity of Θ forces any two harmonic modes $\vec{H}_1(r)$ and $\vec{H}_2(r)$ with different frequencies ω_1 and ω_2 to have an inner product of zero:

   It has been already known that $\Theta\vec{H}_1(r) = \left(\frac{\omega_1}{c}\right)^2 \vec{H}_1(r)$ and $\Theta\vec{H}_2(r) = \left(\frac{\omega_2}{c}\right)^2 \vec{H}_2(r)$. Therefore $(\vec{H}_2, \Theta\vec{H}_1) = \left(\frac{\omega_1}{c}\right)^2 (\vec{H}_2, \vec{H}_1) = (\Theta\vec{H}_2, \vec{H}_1) = \left(\frac{\omega_2}{c}\right)^2 (\vec{H}_2, \vec{H}_1)$. If $\omega_1 \neq \omega_2$, then we must have $(H_2, H_1) = 0$ which means that H_1 and H_2 are orthogonal modes.

4.3.4 Electromagnetic Energy and Variational Principle

Electromagnetic energy functional $E_f$is defined as follows:

$$E_f = \frac{1}{2}\frac{(\vec{H}, \Theta\vec{H})}{(\vec{H}, \vec{H})} \tag{4.69}$$

If we substitute (4.68) into (4.69), we get

$$E_f = \left(\frac{1}{2}\frac{1}{(\vec{H}, \vec{H})}\right) \int dr \frac{1}{\epsilon} \left|\nabla \times \vec{H}\right|^2 = \left(\frac{1}{2}\frac{1}{(\vec{H}, \vec{H})}\right) \int dr \frac{1}{\epsilon} \left|\frac{\omega}{c}\vec{D}\right|^2 \tag{4.70}$$

From this expression it can be seen that E_f is minimized when the displacement field $\vec{D}$ is concentrated in the regions of high dielectric constant. To minimize E_f, a harmonic mode will therefore tend to concentrate its displacement field in regions of high dielectric, while remaining orthogonal to the modes below it in frequency [26].

4.3.5 Time Reversal Symmetry

If we take the complex conjugate of the master equation (4.6), and use the fact that the eigenvalues are real, we obtain:

$$(\Theta\vec{H}_{kn})^* = \frac{\omega_n^2(k)}{c^2}\vec{H}_{kn}^* \tag{4.71}$$

$$\Theta\vec{H}_{kn}^* = \frac{\omega_n^2(k)}{c^2}\vec{H}_{kn}^* \tag{4.72}$$

By this derivation we see that $\vec{H}^*_{kn}$ satisfies the same equation as $\vec{H}_{kn}$ with the same eigenvalue. In addition, from Bloch-Floquet's theorem, we know that $\vec{H}^*_{kn}$ is just the Bloch state at $(-k, n)$ (see (4.18)). Therefore it can be concluded that

$$\omega_n(k) = \omega_n(-k) \tag{4.73}$$

The above relation holds for any photonic crystal. The frequency bands have inversion symmetry even if the crystal does not. Taking the complex conjugate of $\vec{H}_{kn}$ is equivalent to reversing the sign of time t in the Maxwell's equations. Therefore, we can say that (4.73) is a consequence of the time-reversal symmetry of the Maxwell's equations.

Chapter 5

SUMMARY OF RESEARCH

The main goal of this research was to gain a complete understanding of planar layered medium including its electromagnetic wave nature, design and analysis methods. In order to achieve this understanding, we studied specific application of layered media especially used by today's technology and exciting the researchers with their possible future applications. First one of these planar layered structures was chirped mirrors. After the sole trade of prism pairs, chirped mirrors opened the way of obtaining more stable short-pulse laser with higher performance by compensating the dispersion. In this thesis we considered dispersion concept and designed a chirped mirror exhibiting high reflectivity and desired GDD and reviewed the design algorithm. In addition, as a possible extension of this study for future work, the optimization can be also applied to reduce GDD fluctuations in a broader frequency range.

The second layered media application, that we have paid attention, were one dimensional photonic crystals. Before taking only one dimensional case, we studied photonic crystals first in general to understand the periodicity effects on its electromagnetic analysis. Therefore we reviewed both one and two dimensional photonic crystals by analyzing them with plane wave method. Then we proposed a new analysis method, namely GPOF approach, to obtain the dispersion characteristics of one dimensional photonic crystals which is an alternative approach to plane wave method. This approach finds $\omega - k$ diagram of the photonic crystal in a more realistic manner since photonic crystals to be analyzed has limited layers. The analysis results found by both method are demonstrated for comparison purposes. In addition, with GPOF approach, we found effective permittivity and permeability of the crystal so we could model it as if it were a homogeneous material. In addition, the ability of the method to analyze dispersion relations for oblique incident waves is investigated, as well. As a future study, this method can give us an opportunity to extend the idea for higher dimensional photonic crystals.

BIBLIOGRAPHY

[1] Ch. Spielmann, P.F.Curley, T. Brabec,F.Krausz, IEEE J. Quantum Electron.**30**,1100 (1994)

[2] R. Szipöcs, K. Ferencz, C. Spielmann, and F. Krausz, Opt. Lett. **19**,201(1994)

[3] J. H. Holland, "Adaptation in Natural and Artificial Systems: An Introductory Analysis with Applications to Biology, Control, and Artificial Intelligence". Ann Arbor, MI:University of Michigan Press, (1975).

[4] E. Yablonovitch, "Inhibited spontaneous emission in solid-state physics and electronics", Phys. Rev. Lett.,vol. **58**,no. 20, pp. 20592062, May 1987.

[5] S. John, "Strong localization of photons in certain disordered dielectric superlattices", Phys. Rev. Lett., vol.**58**, no.23, pp. 24862489, June 1987

[6] J. Sabarinathan et al. "An electrically injected InAs/GaAs quantum-dot photonic crystal microcavity light-emitting diode", Applied Physics Letters **81**, 3876-3878 (2002).

[7] Mekis, A. et al. "High transmission through sharp bends in photonic crystal waveguide". Phys.Rev.Lett. **77**, 3787 (1996).

[8] Soljacic, M., Ibanescu, M., Johnson, S. G., Fink, Y. Joannopoulos, J. D. "Optimal bistable switching in nonlinear photonic crystals". Physical Review E: Statistical, Nonlinear, and Soft Matter Physics **66**, 055601/1-055601/4 (2002).

[9] K. M. Leung and Y. F. Liu, "Full vector calculation of photonic band structures in face-centered-cubic dielectric media", Physical Review Letters, vol. **65**, no. 21, pp. 26462649, Nov 1990.

[10] Z. Zhang and S. Satpathy, "Electromagnetic wave propagation in periodic structures: bloch wave solution of Maxwells equations", Physical Review Letters, vol.**65**, no. 21, pp. 26502653, Nov 1990.

[11] K. M. Ho, C. T. Chan, and C. M. Soukoulis, "Existence of a photonic gap in periodic dielectric structures", Physical Review Letters, vol. **65**, no. 25, pp. 31523155, Dec 1990.

[12] R. L. Fork et al., "Negative dispersion using pairs of prisms", Opt. Lett. **9**,150 (1984)

[13] F. X. Kärtner, N. Matuschek, T. Schibli, U. Keller, H. A. Haus, C. Heine, R. Morf, V. Scheuer, M. Tilsch, T. Tschudi, "Design and fabrication of double-chirped mirrors", Opt. Lett.**22**, 831833, (1997).

[14] N. Matuschek, F. X. Kärtner, U. Keller, "Analytical design of double-chirped mirrors with custom-tailored dispersion characteristics", IEEE J. Quantum Electron. **35**, 129137, (1999).

[15] N. Matuschek, L. Gallmann, D. H. Sutter, G. Steinmeyer, U. Keller "Back-side-coated chirped mirrors with ultra-smooth broadband dispersion characteristics", Appl. Phys. B **71**, 509-522, (2000).

[16] G. Tempea, V. Yakovlev, B. Bacovic, F. Krausz, K. Ferencz, "Tilted-front-interface chirped mirrors", J. Opt. Soc. Am. B **18**, 17471750, (2001).

[17] G. Steinmeyer,"Brewster-angled chirped mirrors for high-fidelity dispersion compensation and bandwidths exceeding one optical octave",Opt. Exp.**11**, 19, 2385-2396, (2003).

[18] R.Szipöcs and A. Kohazi-Kis,"Theory and design of chirped dielectric laser mirrors",Appl.Phys.B **65**,115-145(1997).

[19] T. A. Birks, J. C. Knight, and P. St. J. Russell, "Endlessly single-mode photonic crystal fiber", Opt. Lett., vol.**22**, pp. 961963, July 1997.

[20] J. C. Knight, J. Broeng, T. A. Birks, and P. St. J. Russell, "Photonic band gap guidance in optical fibers", Science, vol. **282**, pp. 14761478, Oct. 1998.

[21] J. Broeng, D. Mogilevtsev, S. E. Barkou, and A. Bjarklev, "Photonic crystal fibers: A new class of optical waveguides", Opt. Fiber Technol., vol.**5**, pp. 305330, July 1999.

[22] J. Broeng, S. E. Barkou, and A. Bjarklev, "Analysis of air-guiding photonic bandgap fibers", Opt. Lett., vol.**25**, Jan. 2000.

[23] Artificial Intelligence, Structures and Strategies for Complex Problem Solving, Fourth Edition, at page 471. Luger, George F. 2002. Harlow, England: Addison-Wesley.

[24] NIMs NOW, "Fabrication Techniques for 3-Dimensional Photonic Crystals", Materials Research Supporting Innovative Optical Technology, National Institude for Material Science, Sep.2006

$< http://www.nims.go.jp/eng/news/nimsnow/Vol2/No5/p1.html >$.

[25] De Dood, M., "Photonic Crystals", Homepage-Michiel De Dood, Aug. 1998, Sep. 2006 $< http://www.dedood.demon.nl/PhotonicCrystals.html >$.

[26] J. D. Joannopoulos, R. D. Meade, and J. N. Winn,"Photonic Crystals: Molding the Flow of Light", Princeton University Press, Princeton, 1995.

[27] J. D. Joannopoulos, P. R. Villeneuve, and S. Fan, "Photonic crystals: Putting a new twist on light", Nature, vol. **386**, pp. 143149, Mar. 1997.

[28] J. D. Joannopoulos, R. D. Meade, and J. N. Winn, "Photonic Crystals: Molding the Flow of Light", Princeton University Press, Princeton,p. 44, 1995.

[29] Y. Hua and T. K. Sarkar, "Generalized pencil-of-function method for extracting poles of an EM system from its transient response", IEEE Trans. Antennas Propagat., vol. **37**, pp. 229-234, Feb. 1989.